Construction and Validation of a Ferroptosis-Related Prognostic Signature in Kidney Renal Clear Cell Carcinoma

Zhuolun Sun
Third Affiliated Hospital of Sun Yat-Sen University https://orcid.org/0000-0003-2021-2775
Changying Jing
Shandong University of Traditional Chinese Medicine
Chutian Xiao
Third Affiliated Hospital of Sun Yat-Sen University
Mingxiao Zhang
Third Affiliated Hospital of Sun Yat-Sen University
Zhenqing Wang
Third Affiliated Hospital of Sun Yat-Sen University
Mingzhao Li
Third Affiliated Hospital of Sun Yat-Sen University
Hua Wang (TigerS323@163.com)
Third Affiliated Hospital, Sun Yat-sen University https://orcid.org/0000-0001-7110-3697

Primary research

Keywords: Kidney renal clear cell carcinoma (KIRC), The Cancer Genome Atlas (TCGA), The International Cancer Genome Consortium (ICGC), Ferroptosis-related gene (FRG), Prognostic signature, Overall survival (OS), Nomogram

Posted Date: November 17th, 2020

DOI: https://doi.org/10.21203/rs.3.rs-105339/v1

Abstract

Background: Kidney renal clear cell carcinoma (KIRC) is the most common and lethal renal cell carcinoma (RCC) histological subtype. Ferroptosis is a newly discovered programmed cell death and serves an essential role in tumor occurrence and development. The purpose of this study is to analyze ferroptosis-related gene (FRG) expression profiles and to construct a multi-gene signature for predicting the prognosis of KIRC patients.

Methods:

RNA-sequencing data and clinicopathological data of KIRC patients were downloaded from The Cancer Genome Atlas (TCGA). Differentially expressed FRGs between KIRC and normal tissues were identified using 'limma' package in R. GO and KEGG enrichment analyses were conducted to elucidate the biological functions and pathways of differentially expressed FRGs. Consensus clustering was used to investigate the relationship between the expression of FRGs and clinical phenotypes. Univariate and the least absolute shrinkage and selection operator (LASSO) Cox regression analysis were used to screen genes related to prognosis and construct the optimal signature. Then, a nomogram was established to predict individual survival probability by combining clinical features and prognostic signature.

Results: A total of 19 differentially expressed FRGs were identified. Consensus clustering identified two clusters of KIRC patients with distinguished prognostic. Functional analysis revealed that metabolism-related pathways were enriched, especially lipid metabolism. A 7-gene ferroptosis-related prognostic signature was constructed to stratify the TCGA training cohort into high- and low-risk groups where the prognosis was significantly worse in the high-risk group. The signature was identified as an independent prognostic indicator for KIRC. These findings were validated in the testing cohort, the entire cohort, and the International Cancer Genome Consortium (ICGC) cohort. We further demonstrated that the signature-based risk score was highly associated with the KIRC progression. Further stratified survival analysis showed that the high-risk group had a significantly lower overall survival (OS) rate than those in the low-risk group. Moreover, we constructed a nomogram that had a strong ability to forecast the OS of the KIRC patients.

Conclusion: We constructed a ferroptosis-related prognostic signature, which might provide a reliable prognosis assessment tool for clinician to guide clinical decision-making and outcomes research.

Background

Renal cell carcinoma (RCC) is one of the most common tumors in the urinary system and accounts for approximately 3% of all adult malignancies in western countries[1]. The incidence of RCC is increasing at an annual rate of 3–5%, with an estimated 140,000 kidney cancer-related deaths per year[2, 3]. Kidney renal clear cell carcinoma (KIRC) is the most common and lethal subtype of RCC, accounting for 90% of all kidney cancers[4]. Despite improvements in the surgery and other comprehensive treatment methods, the clinical outcomes for KIRC remain unsatisfactory, with a median overall survival (OS) of 21.4 months[5]. Surgical resection remains the definitive treatment for patients with localized disease. Approximately 30% of patients present metastatic at the time of diagnosis, which requires systemic therapies and is associated with high mortality[6]. The complex etiologic factors, along with the high-level heterogeneity of KIRC, makes prognostication and choice of treatment strategy difficult[7]. In KIRC patients, the tumor grade at the time of diagnosis may affect the survival rate. The 5-year tumor-specific mortality rate for grade 1 patients is about 7%, and that for grade 4 patients is about 58%[8]. Therefore, to

improve the therapeutic outcomes and life quality of patients, there is an additional need for developing more effective biomarkers for early screening and diagnosis.

Programmed cell death (PCD) is a fundamental self-destruction process in cell development and growth, which is widely considered a positive process that both prevents and treats cancer[9]. However, abundant studies have demonstrated that PCD can also cause unwanted effects that may even promote tumorigenesis, progression, and metastasis[10–12]. Ferroptosis is a newly discovered form of PCD characterized by iron-dependent lipid peroxide accumulation, and distinct from traditional apoptosis or autophagic cell death or necrosis[13]. Ferroptosis is closely related to the metabolism of iron, fatty acids, amino acids, as well as the biosynthesis of glutathione, phospholipids, and NADPH[14, 15]. Given that the iron-dependent accumulation of lipid reactive oxygen species (ROS) kills cells undergoing ferroptosis, both iron metabolism and lipid peroxidation are two critical processes involved in the mechanism of ferroptosis[16]. Preliminary evidence suggests that may ferroptosis may have a tumor suppressor function that could be potentially beneficial for cancer therapy[14]. On the other hand, various studies have also confirmed the pivotal role of ferroptosis in tumor development[17–19]. For example, Guerriero et al. evaluated the GPX4 expression in hepatocellular carcinoma tissue samples and verified that GPX4 was significantly over-expression and associated with an increased malignancy grade[20]. There is longstanding evidence that various primary tumors and also metastases express DPP4 to a variable extent[21]. In addition, other ferroptosis regulatory genes such as S1R[22], NRF2[23], and HSPB1[24] have also been shown to be strongly correlated with the tumorigenesis and progression. However, whether these ferroptosis-related genes (FRGs) are correlated with the prognosis of KIRC patients has not been investigated in detail.

In the present study, we first performed a genome-wide comparative analysis of FRGs expression profiles and investigated differentiated FRGs expression patterns in KIRC patients based on the data obtained from The Cancer Genome Atlas (TCGA). Subsequently, we conducted functional enrichment analysis for these aberrantly expressed FRGs to systematically explored their potential functions and molecular mechanisms. After Cox univariate analysis and least absolute shrinkage and selection operator (LASSO) Cox regression analysis, we constructed a 7-gene signature with the ability to predict the prognosis of patients with KIRC in the training cohort and validated its prognostic value in the testing cohort, the entire cohort, and the ICGC cohort. Univariate and multivariate survival analysis indicated that the signature could serve as an independent factor for KIRC patients. Moreover, we developed a novel promising prognostic nomogram model with more accurate predictive ability by combining the ferroptosis signature and clinical parameters. Overall, our results demonstrate that some FRGs play vital roles in KIRC progression and are potential prognostic markers and therapeutic targets for KIRC.

Materials And Methods

Data acquisition

We downloaded the RNA-sequencing dataset of 72 normal kidney tissue samples and 539 KIPC samples with corresponding clinical data from The Cancer Genome Atlas (TCGA, https://cancergenome.nih.gov/) database. We excluded cases (n = 5) without follow-up records (survival time code of 0 months). Patients (n = 48) with incomplete clinical data were excluded from this analysis. RNA-seq data and clinical information of another 90 KIRC were obtained from The International Cancer Genome Consortium (ICGC, https://dcc.icgc.org/) data portal, which were used as an independent external validation set. Ethics approval and informed consent were not required for this study because the data from TCGA and ICGC were both publicly available. In addition, our research followed the access rules and publication guidelines provided by the TCGA and ICGC.

We searched the previous literature to identify 61 ferroptosis-related genes (FRGs) described so far to be involved in ferroptosis[14, 19, 25], and the gene sets of the ferroptosis process were shown in Additional file 1: Table S1. The expression data of the FRGs were extracted and used for subsequent analysis.

Data preprocessing and differentially expressed FRGs screening in KIRC

All the raw expression data were subject to quality control, background correction, normalization, and logarithmic conversion by the R language (version 4.0.1, http://www.r-project.org/) [26] or Practical Extraction and Reporting Language (PERL, version 5.30.2, http://www.perl.org) [27]. The ensemble gene IDs were then converted to gene symbols using the GRCh38 reference genome (http://asia.ensembl.org/index.html) in this study. The FRGs that were differentially expressed between the tumor and normal samples were then identified based on a threshold of |logFC (fold change)| > 1 and a false discovery rate (FDR) < 0.05. Next, a Protein-Protein Interaction (PPI) network of the differentially expressed FRGs was generated by the Search Tool for the Retrieval of Interacting Genes (STRING, http://string.embl.de/) [28]. Visualization was then rendered using Cytoscape (http://www.cytoscape.org/) [29].

Functional enrichment analyses

The biological functions of these differently expressed FRGs were comprehensively detected by gene ontology (GO) enrichment, which comprised three terms: biological process (BP), cellular component (CC), and molecular function(MF). The Kyoto Encyclopedia of Genes and Genomes database (KEGG) was applied to explore the significant pathways of differentially expressed FRGs. All enrichment analyses were carried out by utilizing the 'ClusterProfiler' R package [30]. Both *P* and FDR values < 0.05 were considered to be statistically significant.

GSCALite (http://bioinfo.life.hust.edu.cn/web/GSCALite/) database was a web-based analysis platform for gene set cancer analysis, which can help cancer research community to discovery cancer pathways and drugs [31]. In the current research, we also used the GSCALite database to analyze degree of the genes activation or inhibition of the classical pathway.

Non-negative matrix factorization consensus clustering

To investigate the relationship between the expression of FRGs and clinical phenotypes in KIRC, we clustered KIRC cohort from TCGA into different clusters by consensus expression of FRGs with 'ConsensusClusterPlus' in R [32]. Principal component analysis (PCA) was carried out to evaluate the gene expression patterns in the different subgroups. We also compared the OS difference between different clusters by the Kaplan-Meier method in R. Chi-square test was used to compare the frequency distribution of age, gender, grade, AJCC (The American Joint Committee on Cancer) stages, TNM (Tumor, Node, Metastasis) stages between different clusters. N stage was not analyzed because of a large proportion of missing data.

Construction and validation of the ferroptosis-related prognostic risk signature

The expression data of the differentially expressed FRGs were explored using the univariate Cox regression analysis to screen ferroptosis-related genes with prognostic values ($P < 0.05$). The TCGA-KIRC dataset was then randomly divided into a training cohort (n = 294) and a testing cohort (n = 192) for subsequent validation. To control the complexity of the model and avoid overfitting, the least absolute shrinkage and selection operator (LASSO) Cox regression was performed to construct a prognostic signature within the training cohort [33]. We repeated the simulations 1000 times for which the optimal penalty parameter (λ) was selected through 10-fold cross validation following the minimum criteria. In addition, only genes with non-zero coefficients in the LASSO Cox regression were

chosen to further calculate the risk score [34]. The risk score was estimated using the following formula: Risk Score. N, Expi, and Coei represented gene number, level of gene expression, and coefficient value, respectively. The median risk score was chosen as a cutoff value to dichotomize the training cohort into high-risk and low-risk groups. The Kaplan–Meier survival curve was plotted to evaluate the differences in OS between the two groups by the log-rank test. Additionally, the receiver operating characteristic (ROC) curve and the area under the ROC curve (AUC value) were used to evaluate the accuracy of the prognostic signature. Univariate and multivariate Cox regression analyses were used to determine whether risk score was an independent prognostic factor. For the survival analysis of each gene in the signature, the optimal cut-off expression value was determined using the X-Tile software[35]. Besides, the testing cohort, the entire cohort, and the ICGC cohort were used as validation cohorts to confirm the predictive capability of this prognostic signature using the same formula.

The clinical utility of the prognostic risk signature

To test the usability and feasibility of the signature in the clinic, the associations between the ferroptosis-related risk signature and clinicopathologic features in TCGA-KIRC patients were performed. Using the Kaplan-Meier survival curves, we explored the ability of the prognostic risk signature to predict the survival outcomes of KIRC patients stratified by various clinicopathological characteristics, including age (≤ 60 and > 60), gender (female and male), grade(G1-2 and G3-4), AJCC stage(Ⅰ/Ⅱ and Ⅲ/Ⅳ), T stage (T1-2 and T3-4), and M stage (M0 and M1).

In addition to this, a nomogram, integrated the prognostic signature and clinical parameters, was constructed as a quantitative prediction tool to evaluate clinical prognosis. Following that, calibration curves were generated to evaluate the concordance between actual and predicted survival. Moreover, the concordance index (C-index) was computed to assess the model performance for predicting prognosis, with a C-index of 1 indicating perfect discrimination and a C-index 0.5 indicating a random guess. Decision curve analysis (DCA) was performed by calculating the net benefits for a range of threshold probabilities to estimate the clinical usefulness of the nomogram.

The expression patterns, SNVs, CNVs, and drug sensitivity of the genes in the signature

In order to confirm the reliability of the genes in the signature, we verified the expression patterns in different pathological tumors based on the data from the TCGA database. GSCALite database was used to analyze single nucleotide variations (SNVs) and copy number variations (CNVs) of the genes in the signature in KIRC patients.

CellMiner (https://discover.nci.nih.gov/cellminer/home.do) was used to detect the levels of the signature-related genes in the different renal cancer cells and the resulting values were represented as a heatmap. To provide support for drug selection of gene targeting therapy, we then analyzed the correlation of gene expression and drug sensitivity in KIRC patients with GSCALite database.

Results

Differentially expressed FRGs in KIRC

Using transcriptome data from the TCGA database, we analyzed the mRNA levels of 61 FRGs in KIRC and normal tissues. A total of 19 differentially expressed FRGs were eventually identified using the criteria of |log2FC| > 1 and FDR < 0.05, including 13 downregulated genes (MT1G, ACSF2, CHAC1, ACSL4, AKR1C2, PEBP1, PTGS2, AKR1C1, CBS, GOT1, ACO1, FDFT1, and HMGCR) and 6 upregulated genes (ALOX12, CD44, SLC7A11, ALOX5, HMOX1, and

ALOX15B) in KIRC tissues compared to the normal kidney tissues (Fig. 1a, b). The box diagram was utilized to exhibit the expression patterns, median values, and data ranges of the differentially expressed FRGs in tumor and normal samples (Fig. 1c). The interaction network among these genes was presented in Fig. 1d, and the result indicated that PTGS2 and HMOX1 seemed to be the hub genes in this network.

Two ferroptosis subgroups were different in clinical phenotypes and OS via consensus clustering analysis

According to expression levels of 61 FRGs, the total TCGA-KIRC cohort was clustered into 2 subgroups (cluster 1 and cluster 2) with k = 2 as the optimal value because the grouping was suboptimal when they were divided into more than 2 clusters (Fig. 2a-c). Moreover, principal component analysis (PCA) was performed to compare the transcriptional profile between cluster 1 and cluster 2. The result demonstrated that there was a significant distinction between the two subgroups (Fig. 2d). To better understand the clustering result and its relationships with survival outcomes, we compared the OS between cluster 1 and cluster 2 and observed cluster 2 had shorter OS than cluster 1 for the KIRC patients (Fig. 2e). We then evaluated associations between the clustering and the clinicopathological parameters of KIRC patients. The result showed that these 2 clusters were different in grade ($P < 0.05$), AJCC stage ($P < 0.001$), T stage ($P < 0.01$), N stage ($P < 0.01$), and survival status ($P < 0.05$), but did not show any significant differences in age and gender (Fig. 2f). Therefore, these results suggested that ferroptosis was closely related to clinical phenotypes and the progression of KIRC.

Functional Enrichment Analyses Of The Differentially Expressed Frgs

To elucidate the biological functions and pathways of the 19 differentially expressed FRGs, GO functional annotation and KEGG pathway enrichment analyses were conducted. The results indicated that these differently expressed FRGs were significantly enriched in the biological process (BP) related to several metabolic process, such as cofactor metabolic process, fatty acid metabolic process, and fatty acid derivative metabolic process (Fig. 3a, b). Furthermore, lipoxygenase pathway was also involved. In terms of molecular function (CC), we found that the differently expressed FRGs were significantly enriched in peroxisomal membrane, microbody membrane, and caveola. Through the molecular function (MF), the differently expressed FRGs were notably enriched in oxidoreductase activity, dioxygenase activity, and lyase activity. In the KEGG pathway enrichment analysis, these genes were shown to be mostly associated with pathways in arachidonic acid metabolism, serotonergic synapse, and ferroptosis (Fig. 3c, d). In addition, we explored the effect of the differentially expressed FRGs in multiple classical signaling pathways on KIRC using the GSLA database. The results revealed that some FRGs was associated with the activation or inhibition of oncogenic pathways. For example, SLC7A11 expression was related to the activation of apoptotic, cell cycle, and EMT pathways; PTGS2 expression was related to the inhibition of cell cycle, DNA damage response, hormone AR, and hormone ER (Additional file 2: Figure S1).

Prognosis-related FRDs selecting and construction of a prognostic signature based on seven FRGs in the TCGA training cohort of KIRC patients

We conducted a univariate Cox regression analysis on the transcriptome data from the TCGA-KIRC dataset and found that the expression of 11 FRGs (CBS, GOT1, FDFT1, HMOX1, CD44, ACO1, AKR1C2, PEBP1, CHAC1, HMGCR, and SLC7A11) was significantly related to the KIRC survival ($P < 0.05$; Fig. 4a). Genes (CBS, CD44, AKR1C2, CHAC1, and SLC7A11) with HR > 1 were considered as risk genes, while the remaining six genes (GOT1, FDFT1, HMOX1, ACO1, PEBP1, and HMGCR) with HR < 1 as protective genes. Based on the expression profile of the 11 genes mentioned above in the training cohort, a prognostic risk signature was constructed by the least absolute shrinkage and selection operator (LASSO) Cox regression analysis. As a result, a 7-gene signature (CBS, HMOX1, CD44, AKR1C2, CHAC1, HMGCR, and SLC7A11) was identified based on the optimal value of λ (Fig. 4b, 4c). Survival analyses based on the optimal cut-off expression value of each gene showed that high expression of risk genes (CBS, CD44, AKR1C2, CHAC1, and SLC7A11) was correlated with poor prognosis, while high expression of protective genes (HMOX1 and HMGCR) displayed the opposite patterns (Additional file 3: Figure S2).

Based on the 7 candidate FRGs, the risk score of each patient was calculated according to the following formula: Risk score = (3.8463 × CBS) + (-0.0021 × HMOX1) + (0.0101 × CD44) + (0.0208 × AKR1C2) + (0.0252 × CHAC1) + (-0.1354 × HMGCR) + (0.3774 × SLC7A11). We then used the median risk score as a cutoff point for classifying KIRC patients in the training cohort (n = 294) into high-risk group (n = 147) and low-risk group (n = 147). Kaplan-Meier survival curve analysis showed that OS was significantly different between the predicted two risk groups and the high-risk group had significantly shorter survival time compared to low-risk group ($P = 4.709e\text{-}06$; Fig. 4d). The survival rates at three and five years in the high-risk group were 61.9% and 49.2%, respectively, while the corresponding rates in the low-risk group were 86.3% and 76.7%, respectively. The ROC curve analysis indicated the risk signature had a promising predictive value for KIRC survival prediction (AUC = 0.734) (Fig. 4e). We then ranked the risk scores of the patients and then analyzed their distributions (Fig. 4f). The distributions of risk scores and the survival status suggested survival rate and time were significantly increased in the low-risk group compared to the high-risk group (Fig. 4g). The heatmap displayed that the expression levels of the 7 candidate FRGs in the high- risk and low-risk groups (Fig. 4h).

Validation of the prognostic signature in the TCGA testing cohort, the TCGA entire cohort, and the ICGC cohort

To verify the accuracy and robustness of the prognostic risk signature, the prognostic value of the signature was further validated in the testing cohort (n = 192), the entire TCGA-KIRC cohort (n = 486). The prognostic risk score was calculated for patients in each cohort based on the prognostic signature. Patients of the testing cohort (n = 192) were stratified into the high-risk group (n = 96) and low-risk group (n = 96) with the median risk score as the cutoff. Similar to the procedure in the entire cohort, the 489 patients of the entire cohort were divided into the high-risk group (n = 243) and low-risk group (n = 243). The detailed clinical features of all KIRC patients were listed in Table 1.

Table 1
Characteristics of KIRP patients included in this study.

Variable	Training cohort (n = 294)	Testing cohort (n = 192)	TCGA cohort (n = 486)	*P*
	Number(%)	Number(%)	Number(%)	
Age				0.9261
≤ 60	148(50.34)	95(49.48)	243(50.00)	
> 60	146(49.66)	97(50.52)	243(50.00)	
Gender				0.6231
Female	102(34.69)	62(32.29)	164(33.74)	
Male	192(65.31)	130(67.71)	322(66.26)	
Grade				0.1454
G1	7(2.38)	3(1.56)	10(2.06)	
G2	125(42.52)	85(44.27)	210(43.21)	
G3	126(42.86)	68(35.42)	194(39.92)	
G4	36(12.24)	36(18.75)	72(14.81)	
AJCC stage				0.9623
□	142(48.3)	94(48.96)	236(48.56)	
□	32(10.88)	18(9.38)	50(10.29)	
□	72(24.49)	48(25)	120(24.69)	
□	48(16.33)	32(16.67)	80(16.46)	
T stage				0.5685
T1	144(48.98)	98(51.04)	242(49.79)	
T2	41(13.95)	20(10.42)	61(12.55)	
T3	101(34.35)	71(36.98)	172(35.39)	
T4	8(2.72)	3(1.56)	11(2.26)	
M stage				0.9837
M0	248(84.35%)	161(83.85%)	409(84.16%)	
M1	46(15.65%)	31(16.15%)	77(15.84%)	

We observed that the results in the testing and entire cohort were consistent with the outcome in the training cohort. Kaplan-Meier survival curves showed that patients in the high-risk group had a significantly worse OS than their low-risk counterparts in both the testing cohort (*P* = 2.149e-08) (Fig. 5a) and the entire TCGA-KIRC cohort (*P* = 7.724e-13) (Fig. 5d). In the testing cohort, the survival rate at 3 years in the high-risk and low-risk group was 65.1% and 87.9%, respectively. The survival rate of high-risk group was 32.4% at 5 years, and that of the low-risk group was 84.8%. Similarly, in the entire TCGA-KIRC cohort, the survival rates at 3 and 5 years in high-risk group were lower than those

in the low-risk group (63.4 vs. 87.7% at 3 years, 41.3 vs. 80.2% at 5 years). ROC curve analysis showed that the AUC values for in the testing cohort and the entire TCGA-KIRC cohort were 0.762 (Fig. 5b) and 0.749 (Fig. 5e), respectively. The risk score distribution, survival status, and the risk gene expression in the testing cohort and the entire TCGA-KIRC cohort were shown in Fig. 5c and 5 f.

Then the prognostic signature was validated in the ICGC cohort (n = 90). Patients were divided into high-risk group (n = 45) and low-risk group (n = 45) with the median risk score. The OS was significantly poorer in the high-risk group than in the low-risk group (*P* = 1.592e-02) (Additional file 4: Figure S3A). The AUC value for the prognostic signature was 0.71, suggesting well-prediction performances (Additional file 4: Figure S3B). The distribution of risk score, survival status, and gene expression of KIRC patients in the ICGC cohort was presented in Additional file 4: Figure S3C, which were similar to the above cohorts. Taken together, these results revealed that the risk signature could accurately predict the prognosis of KIPP patients.

The prognostic signature is an independent prognostic factor for KIRC patients

To determine whether the risk signature can be used as an independent prognostic factor, univariate and multivariate Cox regression analyses were performed with the risk score and relevant clinical factors, including age, gender, grade, AJCC stage, T stage, and M stage. In the TCGA training cohort, univariate analyses showed that age and risk score were significantly associated with OS. Besides, subsequent multivariate analyses suggested that age and risk score were still significantly associated with OS (Table 2). Similar results were obtained for both the testing and the entire TGCA-KIRC cohorts (Table 2). Therefore, the risk score calculated based on the prognostic risk signature was an independent adverse prognostic factor for OS in KIRC patients.

Table 2
Univariate and multivariate Cox regression analysis of clinical factors and prognostic risk signature in the training cohort, the testing cohort and the entire cohort.

Variable	Training cohort				Testing cohort				Entire cohort			
	Univariate		Multivariate		Univariate		Multivariate		Univariate		Multivariate	
	HR	*P*	HR	*P*	HR	*P*	HR	*P*	HR	*P*	HR	*P*
Age ≤ 65 vs > 65	1.03	1.23e-03	1.04	1.10e-04	1.03	5.91e-03	1.04	9.28e-04	1.03	1.24e-05	1.04	2.98e-07
Gender Female vs Male	0.95	0.82	1.20	0.43	0.91	0.70	0.78	0.36	0.94	0.70	1.03	0.87
Grade G1-2 vs G3-4	2.05	7.1e-07	1.27	0.16	2.72	3.51e-09	1.67	7.49e-03	2.30	2.24e-14	1.31	3.09e-02
AJCC stage □/□ vs □/□	1.95	3.4e-13	1.75	0.08	1.91	3.42e-09	2.17	8.13e-03	1.93	9.60e-21	1.98	1.40e-03
T stage T1-2 vs T3-4	2.14	2.92e-11	1.00	0.99	1.80	1.35e-05	0.58	4.80e-02	1.99	3.80e-15	0.73	0.11
M stage M0 vs M1	4.07	1.76e-10	0.96	0.94	5.05	8.65e-11	1.38	0.50	4.39	2.68e-19	1.13	0.75
Risk score Low vs High	1.42	6.65e-12	1.46	5.13e-11	1.78	6.33e-08	1.68	4.14e-04	2.08	8.98e-22	2.04	6.91e-14

Prognostic risk score indicated strong associations with clinical characteristics in KIRC

To investigate whether the risk signature could better predict KIPC clinicopathological features, an analysis was performed to explore the associations between the risk signature and clinical parameters. Significant differences were observed between two groups in grade (*P* = 6.264e-06) (Fig. 6a), AJCC stage (*P* = 1.6973-06) (Fig. 6b), T stage (*P* = 4.884e-06) (Fig. 6c), and M stage (*P* = 0.002) (Fig. 6d). Simultaneously, we observed that advanced-stage tumors were significantly associated with the high-risk group, whereas, the early-stage tumors were correlated with the low-risk group.

To detect the prognostic value of our risk score model in different subgroups, we further investigated stratified survival analysis using the following clinical variables: age (≤ 60 and > 60), gender (female and male), tumor grade

(G1-2 and G3-4), AJCC stage (I & II and III & IV), T stage (T1-2 and T3-4), and M stage (M0 and M1). Interestingly, survival analysis indicated the high-risk group had a significantly lower OS rate than those in the low-risk group for all hierarchical cohorts (Fig. 7). Thus, these results suggested that the classification of the risk signature can be used to precisely identify patients with poor prognosis, without the consideration of clinical parameters.

Development Of A Personalized Prognostic Nomogram

A nomogram is a powerful tool that has been extensively applied to quantitatively determine individuals' risk in clinical decision making by incorporating multiple clinical factors [36, 37]. To establish a viable method for predicting survival in patients with KIRC, we developed a prognostic nomogram based on the constructed prognostic risk signature and serval clinical features, including age, gender, grade, AJCC stage, T stage, M stage. The nomogram was devoted to evaluate the probability of 1-, 3-, and 5-year survival (Fig. 8a). Each factor was assigned a score in proportion to its risk contribution to survival in the nomogram. The C-index that was used to evaluate the OS of the nomogram was 0.771. Calibration curves showed optimal agreement when compared with an ideal model (Fig. 8b), particularly for 3- and 5-year survival predicted probabilities. Decision curve analysis (DCA) of the nomogram indicated that the nomogram had a wide and practical range of threshold probability for the TCGA-KIRC cohort for predicting survival rates (Fig. 8c).

The expression patterns, SNVs, CNVs of the seven candidate genes in the signature for KIRC patients

Subsequently, we analyzed the correlation between the expression of each of the seven prognostic risk signature genes and the clinicopathological features of KIRC patients in the TCGA cohort. In terms of grade alone, CBS, CD44, and CHAC1 increased with tumor grade, while HMGCR was decreased. No significantly difference in the expression values of HMOX1, AKR1C2, and SLC7A11 was detected between different tumor grades (Fig. 9a). As for different AJCC stage, CBS, HMGCR, CHAC1, and HMOX1 were significant differentially expressed, with higher expression levels of CBS and CHAC1 indicating higher advanced AJCC stage, while HMGCR and HMOX1 showed the opposite trend (Fig. 9b). Regarding T stage, it was noted that CBS, CD44, CHAC1, and SLC7A1 were significantly up-regulated in advanced T grade, whereas HMGCR was significantly down-regulated (Fig. 9c). CBS, CD44, and HMGCR also represented similar trends in N stage as T stage (Fig. 9d). In general, the expression levels of CBS, CD44, CHAC1, and SLC7A1 were positively correlated with tumor progression, while HMOX1 and HMGCR were negatively correlated with tumor progression, which was consistent with the above study. In addition, AKR1C2 expression appeared to be independent of tumor progression.

We then used the GSCA database to determine the single nucleotide variations (SNVs) of the seven candidate genes in the signature for KIRC patients. The results indicated that the most frequent mutation type was single nucleotide polymorphism (SNP) (Additional file 5: Figure S4A), and missense mutation was the most fraction among these mutations (Additional file 5: Figure S4B). In addition, C > T transversion accounted for the most common of SNV (Additional file 5: Figure S4C). The characteristic of the frequently mutated genes was showed in Additional file 4: Figure S4D. We also analyzed the copy number variations (CNVs) of the seven candidate genes in the signature and found heterozygous mutations (amplification and deletion) in all genes (Additional file 5: Figure S4E).

Drug sensitivity of the seven candidate genes in the signature for KIRC Patients

We next utilized the CellMiner database to explore the expression of seven candidate genes in diverse kidney cancer cell lines, including 786-O, A498, ACHN, CAKI-1, RXF 393, SN12C, UO-31, and TK-10. We observed that the expression levels of these genes showed great heterogeneity in different cell lines (Additional file 6: Figure S5A). In addition, we also investigated the drug sensitivity of the seven candidate genes for the KIRC patients using the GSCALite database. Four of them (CD44, SLC7A11, AKR1C2, and HMOX1) were highly related to drug sensitivity to a number of chemotherapy drugs (Additional file 6: Figure S5B), which provided direct support for drug targeted therapy.

Discussion

It has been previously reported that KIRC is a malignant disease, the pathogenesis may be related to the reprogramming of energetic metabolisms, such as tricarboxylic acid cycle, aerobic glycolysis, amino acids, fatty acids, and dysfunctional oxidative phosphorylation[38, 39]. Ferroptosis is a programmed cell death caused by iron-dependent lipid peroxidation and is different from other types of cell death, including apoptosis[14, 40]. A wide variety of human diseases, including cancer, have been associated with the abnormal function of ferroptosis, and inhibition or upregulation of ferroptosis modulates the metabolic reprogramming of cancer cells [14, 41]. At present, few studies have been performed on ferroptosis in KIRC, and the results also remain controversial[42]. Therefore, investigating the expression patterns of FRGs is critical to understand the role of ferroptosis in KIRC.

In the current study, we systematically investigated the RNA-seq-expression and clinical information of KIRC from the TCGA database. We found that 19 out of 61 FRGs were differentially expressed in KIRC patients, including 6 up-regulated and 13 down-regulated genes. To gain more insights into the functional roles of the differentially expressed FRGs in KIRC, we performed functional enrichment analysis to investigate the associated biological processes and pathways. Functional annotation showed that many biological processes and pathways related to metabolism were enriched, especially lipid metabolism. The current consensus is that the execution of ferroptosis could result from the direct effects of lipid peroxidation[14]. Moreover, the increased lipid peroxidation is a principal mechanistic pathway in renal carcinogenesis induced by different chemicals. Therefore, we have reason to believe that ferroptosis may have a close connection with tumor metabolic reprogramming. We then used consensus clustering analysis to categorize the KIRC cohort into two subgroups (cluster1 and cluster 2) based on the expression of FRGs. Interestingly, the OS was dramatically different between the two subgroups, indicating that the levels of FRGs were closely associated with the prognosis of KIRC patients.

Using Lasso regression and Cox survival analyses, we constructed a risk prognostic signature based on seven prognostic FRGs (CBS, HMOX1, CD44, AKR1C2, CHAC1, HMGCR, and SLC7A11). Every patient with KIRC was assigned into high-risk and low-risk groups according to the prognostic risk signature. We demonstrated that the OS was shorter for the high-risk patients in four cohorts (the training cohort, the testing cohort, the entire TCGA-KIRC cohort, and the ICGC cohort) compared to the low-risk patients. The ROC curves and AUCs indicated that the signature performed well. Recently, more and more studies have suggested that the abnormal expression of the FRGs is involved in human cancer[16, 17, 41]. We further demonstrated that the signature-based risk score was highly associated with the KIRC progression. It was also observed that the risk scores were higher in individuals with more advanced stage disease. Further stratified survival analysis showed that the high-risk group had a significantly lower OS rate than those in the low-risk group for all hierarchical cohorts. In addition, the signature of the seven FRGs was independent of other clinical factors. We also provided a nomogram that reduced the ferroptosis-related signature combined with other clinical parameters into a single numerical estimate of the probability of an event to predict the prognosis of every individual patient. Taken together, these results significantly indicated the potential role of ferroptosis in KIRC.

Our results showed that the expression level of CBS, CD44, AKR1C2, CHAC1, and SLC7A11was positively associated with the progression of KIRC, while contrary results appeared in HMOX1 and HMGCR. Cystathionine *β*-synthase (CBS), a fundamental enzyme in L-cystathionine synthesis, catalyzes the condensation of serine and homocysteine to form cystathionine, which is the initial and rate-limiting step in the transsulfuration pathway[43]. An increasing body of evidence points to the key roles of CBS in tumor progression, such as prostate cancer[44], ovarian cancer[45], and colon cancer[46]. However, another research strongly supports a negative regulatory role for CBS in hepatocellular carcinoma[47]. Thus, the biological function of CBS in cancer is complex and requires further investigation. CD44 is an important cancer stem cell marker in tumors and implicates in malignant processes including cell motility, tumor growth, and angiogenesis[48]. In fact, CD44 has been observed in many human tumors and associated with a poor survival rate[49]. Aldo-Keto reductase 1C2 (AKR1C2), a member of Aldo-Keto reductase subfamily, could mediate similar prostaglandin D2 conversion toward the accumulation of proliferative signals through PI3K/Akt signaling pathway to promote prostate cell proliferation[50]. In addition, Zhang. et al demonstrated that AKR1C2 could act as a targetable oncogene in esophageal squamous cell carcinoma via activating PI3K/AKT signaling pathway. ChaC glutathione-specific γ-glutamyl cyclotransferase 1 (CHAC1) is a proapoptotic γ-glutamyl cyclotransferase that depletes glutathione. There are few studies on CHAC1 at present, and its clinical significances and biological functions in tumors remain unknown. Solute carrier family 7 member 11 (SLC7A11; also known as xCT) is a cystine/glutamate antiporter that imports cystine into the cells while exporting glutamate[51]. SLC7A11 is highly expressed in human tumors, and its overexpression inhibits ROS-induced ferroptosis and abrogates p53(3KR)-mediated tumor growth suppression in xenograft models[52]. Recent studies demonstrated that smoking could induce the expression of SLC7A11 in oral cancer cells, suggesting that overexpression of SLC7A11 may support lung tumor progression[53]. These results suggest that the four genes (CBS, CD44, AKR1C2, and SLC7A11) above are closely related to the occurrence and development of tumors, which are partly consistent with our research.

Heme oxygenase-1 (HMOX-1), a phase II enzyme that responds to electrophilic stimuli, has been reported to play protective or detrimental effects in different diseases, including cancers. HMOX-1 is elevated in a variety of human malignancies, indicating that it contributes to settle the tumor microenvironment for cancer cell growth, angiogenesis, and metastasis[54]. However, emerging evidence has revealed HMOX-1 functions as a negative regulator in erastin- and sorafenib-induced hepatocellular carcinoma and knockdown of HMOX-1 by specific shRNA increased erastin- and sorafenib-induced growth inhibition[23]. Hydroxymethylglutaryl-coenzyme A reductase (HMGCR), the rate-limiting enzyme in the mevalonate pathway, which is generally believed to be a candidate metabolic oncogene[55]. For example, Li. et al found that HMGCR is up-regulated in gastric cancer and promotes the growth and migration of the cancer cells by activating Hedgehog/Gli1 signaling[56]. Interestingly, another study reported that oral atorvastatin and its metabolites are detectable in human breast samples, suggesting that HMGCR may be directly inhibited in breast tumors[57]. It is evident from the above study that HMOX-1 and HMGCR have both tumor-promoting and tumor-suppressive properties. Clearly, further research will be needed to elucidate the role of cancers, especially KIRC.

However, despite these encouraging results, there existed some limitations. Firstly, since the retrospective nature of this study, a multicenter and prospective study is required to assess the potential applicability of our conclusions. Secondly, further studies including *in vivo* and *in vitro* experiments are needed to elucidate the detailed mechanism of key genes for clinical applications. In addition, many prominent prognostic genes in KIRC might have been excluded because merely a single phenotype was considered to construct a prognostic signature in our study.

Conclusion

In conclusion, we provided insights into the roles of FRGs in KIRC and constructed a promising risk prognostic signature that exhibited potential as a biomarker of OS in KIRC patients. The underlying mechanisms whereby differentially expressed FRGs exert their biological roles in metabolism-associated biological processes. We then established a novel promising prognostic nomogram incorporating for providing individualized survival prediction. Therefore, our constructed ferroptosis-related signature is of great clinical importance and may help facilitate personalized medicine in the clinical setting.

Abbreviations

AJCC: The American Joint Committee on Cancer, AUC: area under the curve, BP: Biological processes, CC: Cellular component, C-index: Concordance index, DCA: Decision curve analysis, FRGs: Ferroptosis-related genes, GO: Gene Ontology, GSEA: Gene Set Enrichment Analysis, HR: hazard ratio, ICGC: International Cancer Genome Consortium, KEGG: Kyoto Encyclopedia of Genes and Genomes, KIRC: Kidney renal clear cell carcinoma, LASSO: Least absolute shrinkage and selection operator, MF: Molecular function, OS: Overall survival, PPI: Protein-protein interaction, RBPs: RNA-binding proteins, RCC: Renal cell carcinoma, ROC: Receiver operating characteristic; TCGA: The Cancer Genome Atlas.

Declarations

Acknowledgements

The authors gratefully thank the academic editor and the anonymous reviewers for their insightful comments and suggestions to improve this manuscript.

Authors' contributions

ZS and CJ designed the study, wrote the manuscript, collected the corresponding datasets, and complete in silico analyses. CX, ZW, and MZ assisted in the model construction and model validation. HW and ML supervised the whole project and edited the manuscript. All authors have read and agreed to the published version of the manuscript, contributed to the article and approved the submitted version.

Funding

The study was approved by National Natural Science Foundation of China (81902617).

Availability of data and materials

The datasets used and/or analyzed in the present study are available from the corresponding author on reasonable request.

Ethics approval and consent to participate

Not applicable.

Consent for publication

Not applicable.

Competing interests

The authors declare that they have no competing interests.

References

1. Motzer RJ, Bander NH, Nanus DM. Renal-cell carcinoma. N Engl J Med. 1996;335(12):865–75.
2. Richey SL, Culp SH, Jonasch E, Corn PG, Pagliaro LC, Tamboli P, Patel KK, Matin SF, Wood CG, Tannir NM. Outcome of patients with metastatic renal cell carcinoma treated with targeted therapy without cytoreductive nephrectomy. Annals of oncology: official journal of the European Society for Medical Oncology. 2011;22(5):1048–53.
3. Ferlay J, Soerjomataram I, Dikshit R, Eser S, Mathers C, Rebelo M, Parkin DM, Forman D, Bray F. Cancer incidence and mortality worldwide: sources, methods and major patterns in GLOBOCAN 2012. International journal of cancer. 2015;136(5):E359–86.
4. Hsieh JJ, Purdue MP, Signoretti S, Swanton C, Albiges L, Schmidinger M, Heng DY, Larkin J, Ficarra V. Renal cell carcinoma. Nature reviews Disease primers. 2017;3:17009.
5. Albiges L, Choueiri TK. Renal-cell carcinoma in 2016: Advances in treatment - jostling for pole position. Nature reviews Clinical oncology. 2017;14(2):82–4.
6. Staehler M, Haseke N, Schoeppler G, Stadler T, Gratzke C, Stief CG. Modern Therapeutic Approaches in Metastatic Renal Cell Carcinoma. EAU-EBU Update Series. 2007;5(1):26–37.
7. Ljungberg B, Albiges L, Abu-Ghanem Y, Bensalah K, Dabestani S, Fernández-Pello S, Giles RH, Hofmann F, Hora M, Kuczyk MA, et al. European Association of Urology Guidelines on Renal Cell Carcinoma: The 2019 Update. European urology. 2019;75(5):799–810.
8. Sun M, Lughezzani G, Jeldres C, Isbarn H, Shariat SF, Arjane P, Widmer H, Pharand D, Latour M, Perrotte P, et al. A proposal for reclassification of the Fuhrman grading system in patients with clear cell renal cell carcinoma. European urology. 2009;56(5):775–81.
9. Mishra AP, Salehi B, Sharifi-Rad M, Pezzani R, Kobarfard F, Sharifi-Rad J, Nigam M. Programmed Cell Death, from a Cancer Perspective: An Overview. Mol Diagn Ther. 2018;22(3):281–95.
10. Ichim G, Tait SW. A fate worse than death: apoptosis as an oncogenic process. Nature reviews Cancer. 2016;16(8):539–48.
11. Lee SY, Ju MK, Jeon HM, Jeong EK, Lee YJ, Kim CH, Park HG, Han SI, Kang HS. Regulation of Tumor Progression by Programmed Necrosis. Oxidative Med Cell Longev. 2018;2018:3537471.
12. Mowers EE, Sharifi MN, Macleod KF. Autophagy in cancer metastasis. Oncogene. 2017;36(12):1619–30.
13. Dixon SJ, Lemberg KM, Lamprecht MR, Skouta R, Zaitsev EM, Gleason CE, Patel DN, Bauer AJ, Cantley AM, Yang WS, et al. Ferroptosis: an iron-dependent form of nonapoptotic cell death. Cell. 2012;149(5):1060–72.
14. Stockwell BR, Friedmann Angeli JP, Bayir H, Bush AI, Conrad M, Dixon SJ, Fulda S, Gascón S, Hatzios SK, Kagan VE, et al. Ferroptosis: A Regulated Cell Death Nexus Linking Metabolism, Redox Biology, and Disease. Cell. 2017;171(2):273–85.
15. Xie Y, Hou W, Song X, Yu Y, Huang J, Sun X, Kang R, Tang D. Ferroptosis: process and function. Cell death differentiation. 2016;23(3):369–79.

16. Lu B, Chen XB, Ying MD, He QJ, Cao J, Yang B. The Role of Ferroptosis in Cancer Development and Treatment Response. Front Pharmacol. 2018;8:992–2.
17. Gan B. DUBbing Ferroptosis in Cancer Cells. Cancer research. 2019;79(8):1749–50.
18. Liu HJ, Hu HM, Li GZ, Zhang Y, Wu F, Liu X, Wang KY, Zhang CB, Jiang T. Ferroptosis-Related Gene Signature Predicts Glioma Cell Death and Glioma Patient Progression. Frontiers in cell developmental biology. 2020;8:538.
19. Liang JY, Wang DS, Lin HC, Chen XX, Yang H, Zheng Y, Li YH. A Novel Ferroptosis-related Gene Signature for Overall Survival Prediction in Patients with Hepatocellular Carcinoma. Int J Biol Sci. 2020;16(13):2430–41.
20. Guerriero E, Capone F, Accardo M, Sorice A, Costantini M, Colonna G, Castello G, Costantini S. GPX4 and GPX7 over-expression in human hepatocellular carcinoma tissues. European journal of histochemistry: EJH. 2015;59(4):2540.
21. Enz N, Vliegen G, De Meester I, Jungraithmayr W. CD26/DPP4 - a potential biomarker and target for cancer therapy. Pharmacol Ther. 2019;198:135–59.
22. Bai T, Wang S, Zhao Y, Zhu R, Wang W, Sun Y. Haloperidol, a sigma receptor 1 antagonist, promotes ferroptosis in hepatocellular carcinoma cells. Biochem Biophys Res Commun. 2017;491(4):919–25.
23. Sun X, Ou Z, Chen R, Niu X, Chen D, Kang R, Tang D. Activation of the p62-Keap1-NRF2 pathway protects against ferroptosis in hepatocellular carcinoma cells. Hepatology. 2016;63(1):173–84.
24. Arrigo AP, Gibert B. HspB1 dynamic phospho-oligomeric structure dependent interactome as cancer therapeutic target. Curr Mol Med. 2012;12(9):1151–63.
25. Hassannia B, Vandenabeele P, Vanden Berghe T. Targeting Ferroptosis to Iron Out Cancer. Cancer cell. 2019;35(6):830–49.
26. Null RCTR, Team R, Null RCT, Core Writing T, Null R,., Team R, Null RDCT, Core R, Team R, Team RDC. R: A language and environment for statistical computing. Computing. 2011;1:12–21.
27. Morris JA, Gayther SA, Jacobs IJ, Jones C. A suite of Perl modules for handling microarray data. Bioinformatics. 2008;24(8):1102–3.
28. Szklarczyk D, Franceschini A, Kuhn M, Simonovic M, Roth A, Minguez P, Doerks T, Stark M, Muller J, Bork P, et al. The STRING database in 2011: functional interaction networks of proteins, globally integrated and scored. Nucleic acids research. 2011;39(Database issue):D561–8.
29. Kohl M, Wiese S, Warscheid B. Cytoscape: software for visualization and analysis of biological networks. Methods in molecular biology (Clifton NJ). 2011;696:291–303.
30. Yu G, Wang LG, Han Y, He QY. clusterProfiler: an R package for comparing biological themes among gene clusters. Omics: a journal of integrative biology. 2012;16(5):284–7.
31. Liu CJ, Hu FF, Xia MX, Han L, Zhang Q, Guo AY. GSCALite: a web server for gene set cancer analysis. Bioinformatics. 2018;34(21):3771–2.
32. Wilkerson MD, Hayes DN. ConsensusClusterPlus: a class discovery tool with confidence assessments and item tracking. Bioinformatics. 2010;26(12):1572–3.
33. Sauerbrei W, Royston P, Binder H. Selection of important variables and determination of functional form for continuous predictors in multivariable model building. Statistics in medicine. 2007;26(30):5512–28.
34. Tibshirani R. Regression Shrinkage and Selection Via the Lasso. J Roy Stat Soc B. 1996;58(1):267–88.
35. Camp RL, Dolled-Filhart M, Rimm DL. X-tile: a new bio-informatics tool for biomarker assessment and outcome-based cut-point optimization. Clinical cancer research: an official journal of the American Association for

Cancer Research. 2004;10(21):7252–9.

36. Karakiewicz PI, Briganti A, Chun FK, Trinh QD, Perrotte P, Ficarra V, Cindolo L, De la Taille A, Tostain J, Mulders PF, et al. Multi-institutional validation of a new renal cancer-specific survival nomogram. Journal of clinical oncology: official journal of the American Society of Clinical Oncology. 2007;25(11):1316–22.
37. Liang W, Zhang L, Jiang G, Wang Q, Liu L, Liu D, Wang Z, Zhu Z, Deng Q, Xiong X, et al. Development and validation of a nomogram for predicting survival in patients with resected non-small-cell lung cancer. Journal of clinical oncology: official journal of the American Society of Clinical Oncology. 2015;33(8):861–9.
38. Hakimi AA, Reznik E, Lee CH, Creighton CJ, Brannon AR, Luna A, Aksoy BA, Liu EM, Shen R, Lee W, et al. An Integrated Metabolic Atlas of Clear Cell Renal Cell Carcinoma. Cancer cell. 2016;29(1):104–16.
39. Mulders PF. From genes to metabolomics in renal cell carcinoma translational research. European urology. 2013;63(2):252–3.
40. Yang WS, Stockwell BR. Ferroptosis: Death by Lipid Peroxidation. Trends in cell biology. 2016;26(3):165–76.
41. Wu Y, Zhang S, Gong X, Tam S, Xiao D, Liu S, Tao Y. The epigenetic regulators and metabolic changes in ferroptosis-associated cancer progression. Mol Cancer. 2020;19(1):39.
42. Miess H, Dankworth B, Gouw AM, Rosenfeldt M, Schmitz W, Jiang M, Saunders B, Howell M, Downward J, Felsher DW, et al. The glutathione redox system is essential to prevent ferroptosis caused by impaired lipid metabolism in clear cell renal cell carcinoma. Oncogene. 2018;37(40):5435–50.
43. Zhu H, Blake S, Chan KT, Pearson RB, Kang J. Cystathionine β-Synthase in Physiology and Cancer. BioMed research international. 2018;2018:3205125.
44. Guo H, Gai JW, Wang Y, Jin HF, Du JB, Jin J. Characterization of hydrogen sulfide and its synthases, cystathionine β-synthase and cystathionine γ-lyase, in human prostatic tissue and cells. Urology. 2012;79(2):483.e481-485.
45. Bhattacharyya S, Saha S, Giri K, Lanza IR, Nair KS, Jennings NB, Rodriguez-Aguayo C, Lopez-Berestein G, Basal E, Weaver AL, et al. Cystathionine beta-synthase (CBS) contributes to advanced ovarian cancer progression and drug resistance. PloS one. 2013;8(11):e79167.
46. Phillips CM, Zatarain JR, Nicholls ME, Porter C, Widen SG, Thanki K, Johnson P, Jawad MU, Moyer MP, Randall JW, et al. Upregulation of Cystathionine-β-Synthase in Colonic Epithelia Reprograms Metabolism and Promotes Carcinogenesis. Cancer research. 2017;77(21):5741–54.
47. Kim J, Hong SJ, Park JH, Park SY, Kim SW, Cho EY, Do IG, Joh JW, Kim DS. Expression of cystathionine beta-synthase is downregulated in hepatocellular carcinoma and associated with poor prognosis. Oncol Rep. 2009;21(6):1449–54.
48. Chen C, Zhao S, Karnad A, Freeman JW. The biology and role of CD44 in cancer progression: therapeutic implications. J Hematol Oncol. 2018;11(1):64.
49. Basakran NS. CD44 as a potential diagnostic tumor marker. Saudi Med J. 2015;36(3):273–9.
50. Wang S, Yang Q, Fung KM, Lin HK. AKR1C2 and AKR1C3 mediated prostaglandin D2 metabolism augments the PI3K/Akt proliferative signaling pathway in human prostate cancer cells. Molecular cellular endocrinology. 2008;289(1–2):60–6.
51. Sato H, Tamba M, Kuriyama-Matsumura K, Okuno S, Bannai S. Molecular cloning and expression of human xCT, the light chain of amino acid transport system xc. Antioxid Redox Signal. 2000;2(4):665–71.
52. Jiang L, Kon N, Li T, Wang SJ, Su T, Hibshoosh H, Baer R, Gu W. Ferroptosis as a p53-mediated activity during tumour suppression. Nature. 2015;520(7545):57–62.

53. Ji X, Qian J, Rahman SMJ, Siska PJ, Zou Y, Harris BK, Hoeksema MD, Trenary IA, Heidi C, Eisenberg R, et al. xCT (SLC7A11)-mediated metabolic reprogramming promotes non-small cell lung cancer progression. Oncogene. 2018;37(36):5007–19.
54. Chiang SK, Chen SE, Chang LC. **A Dual Role of Heme Oxygenase-1 in Cancer Cells**. *International journal of molecular sciences* 2018, 20(1).
55. Clendening JW, Pandyra A, Boutros PC, El Ghamrasni S, Khosravi F, Trentin GA, Martirosyan A, Hakem A, Hakem R, Jurisica I, et al: **Dysregulation of the mevalonate pathway promotes transformation**. *Proceedings of the National Academy of Sciences of the United States of America* 2010, **107**(34):15051–15056.
56. Chushi L, Wei W, Kangkang X, Yongzeng F, Ning X, Xiaolei C. HMGCR is up-regulated in gastric cancer and promotes the growth and migration of the cancer cells. Gene. 2016;587(1):42–7.
57. Arun BK, Gong Y, Liu D, Litton JK, Gutierrez-Barrera AM, Jack Lee J, Vornik L, Ibrahim NK, Cornelison T, Hortobagyi GN, et al. Phase I biomarker modulation study of atorvastatin in women at increased risk for breast cancer. Breast cancer research treatment. 2016;158(1):67–77.

Figures

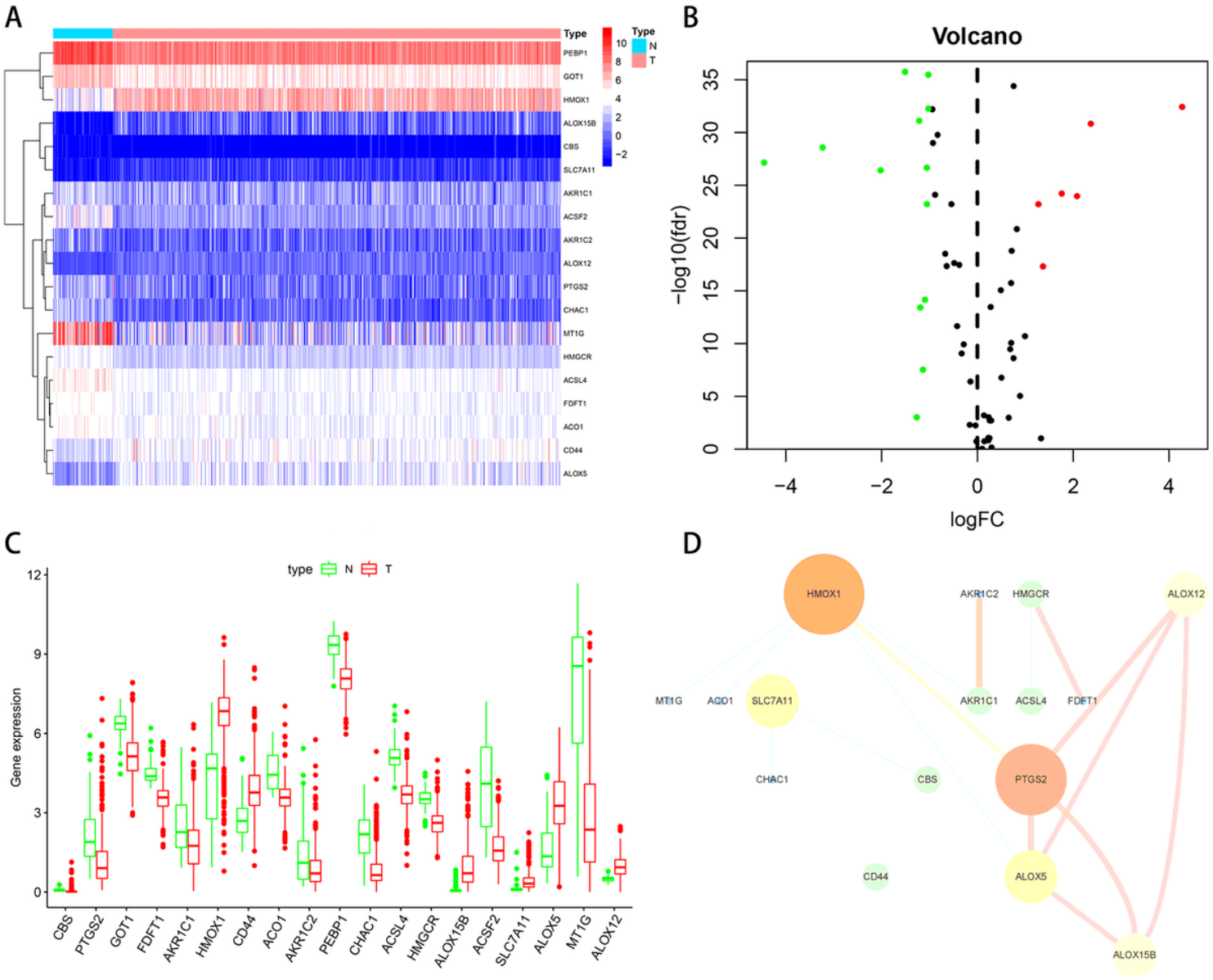

Figure 1

Identification of differentially expressed ferroptosis-related genes (FRGs) in the TCGA-KIRC cohort. (a) The heatmap demonstrates the expression of 19 differentially expressed FRGs in KIRC tissues compared to normal kidney tissues. N and T indicate normal tissues and KIRC tissues, respectively. The color bar from red to blue denotes high to low gene expression. (b) Volcano plot of 19 differentially expressed FRGs in KIRC tissues compared to normal kidney tissues. Red dots represent up-regulated genes, blue dots represent down-regulated genes and black dots represent genes with no significance. (c) The box diagram exhibits the expression patterns, median values and data ranges of the 19 differentially expressed FRGs. (d) The correlation network of the 19 differentially expressed FRGs.

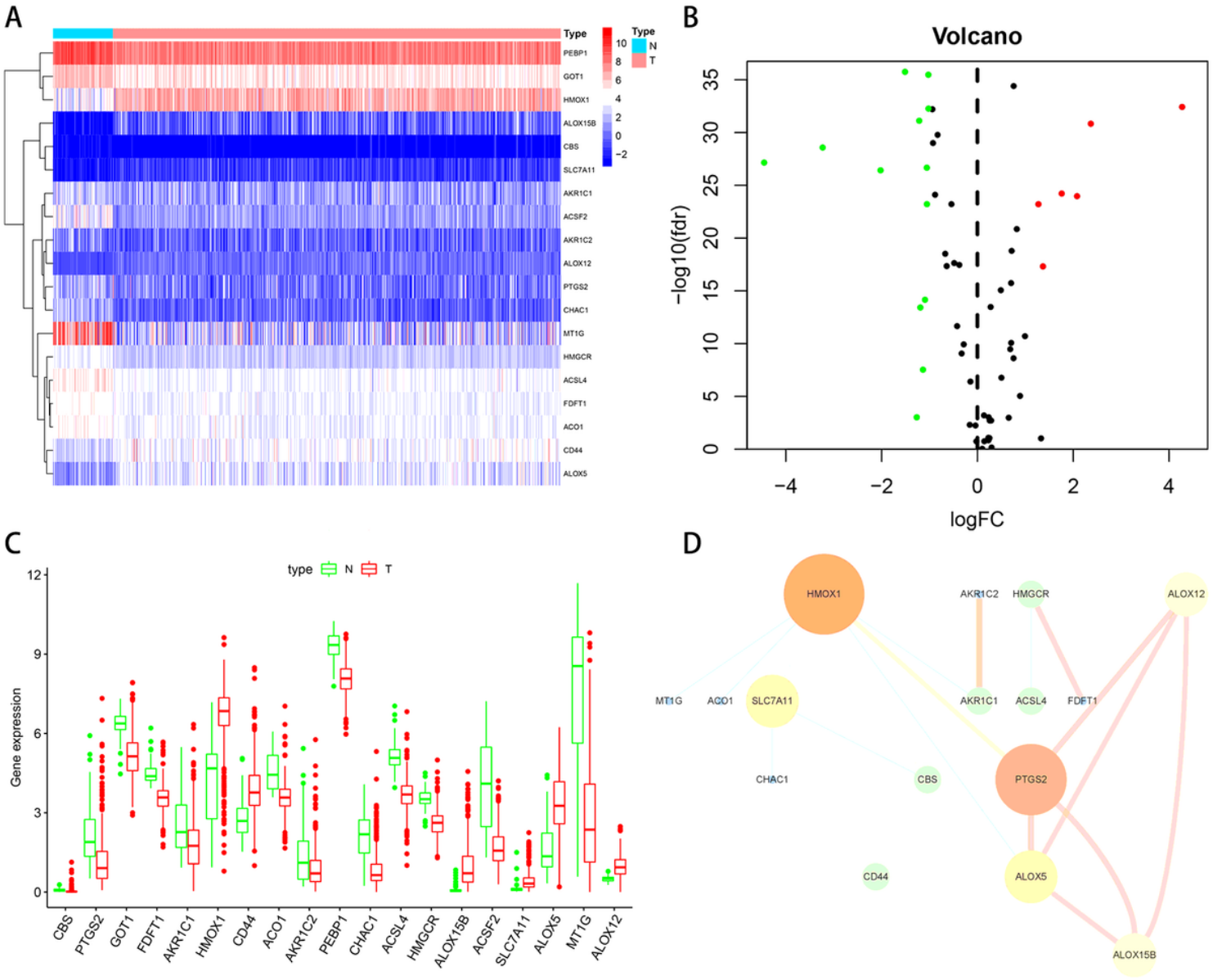

Figure 1

Identification of differentially expressed ferroptosis-related genes (FRGs) in the TCGA-KIRC cohort. (a) The heatmap demonstrates the expression of 19 differentially expressed FRGs in KIRC tissues compared to normal kidney tissues. N and T indicate normal tissues and KIRC tissues, respectively. The color bar from red to blue denotes high to low gene expression. (b) Volcano plot of 19 differentially expressed FRGs in KIRC tissues compared to normal kidney tissues. Red dots represent up-regulated genes, blue dots represent down-regulated genes and black dots represent genes with no significance. (c) The box diagram exhibits the expression patterns, median values and data ranges of the 19 differentially expressed FRGs. (d) The correlation network of the 19 differentially expressed FRGs.

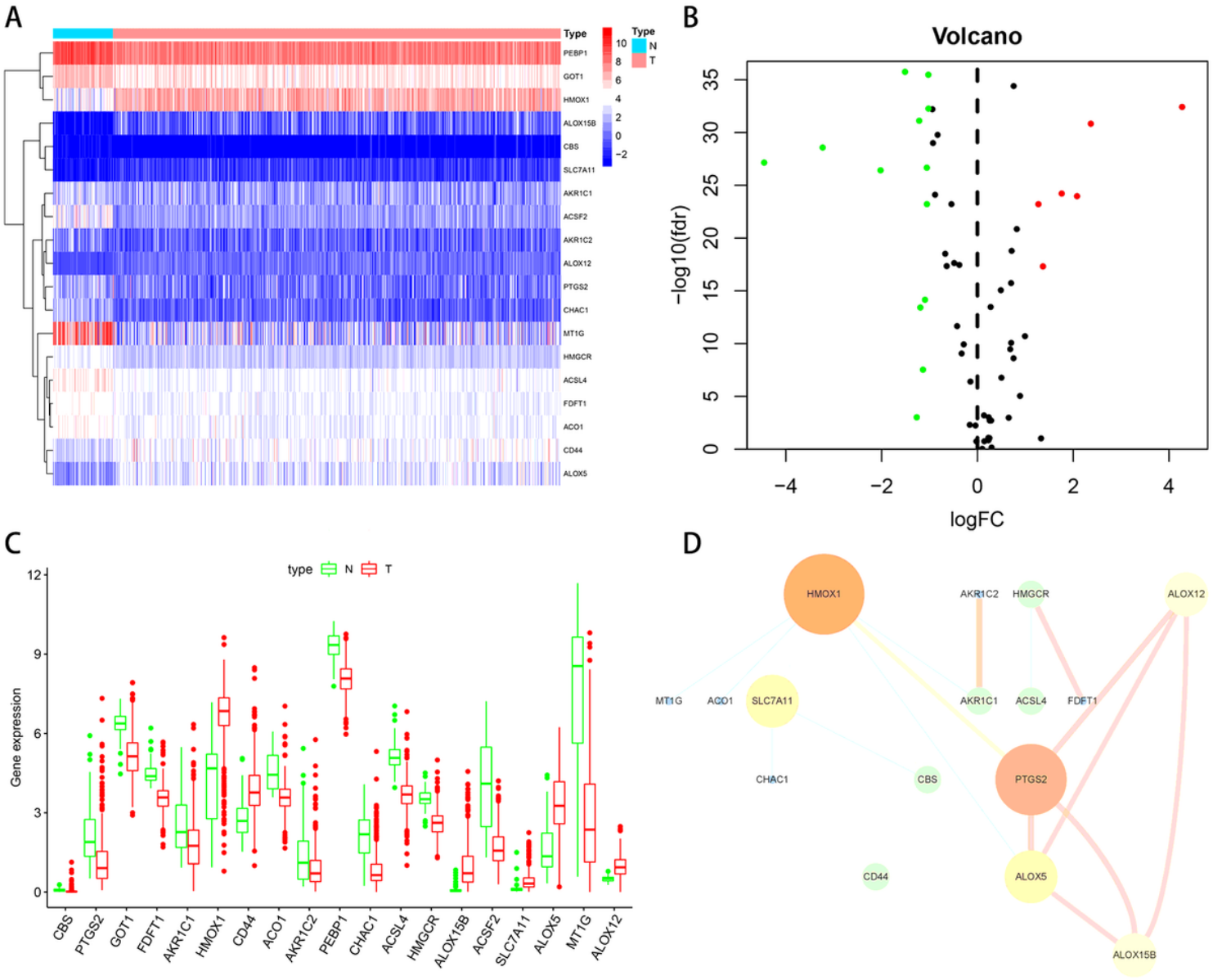

Figure 1

Identification of differentially expressed ferroptosis-related genes (FRGs) in the TCGA-KIRC cohort. (a) The heatmap demonstrates the expression of 19 differentially expressed FRGs in KIRC tissues compared to normal kidney tissues. N and T indicate normal tissues and KIRC tissues, respectively. The color bar from red to blue denotes high to low gene expression. (b) Volcano plot of 19 differentially expressed FRGs in KIRC tissues compared to normal kidney tissues. Red dots represent up-regulated genes, blue dots represent down-regulated genes and black dots represent genes with no significance. (c) The box diagram exhibits the expression patterns, median values and data ranges of the 19 differentially expressed FRGs. (d) The correlation network of the 19 differentially expressed FRGs.

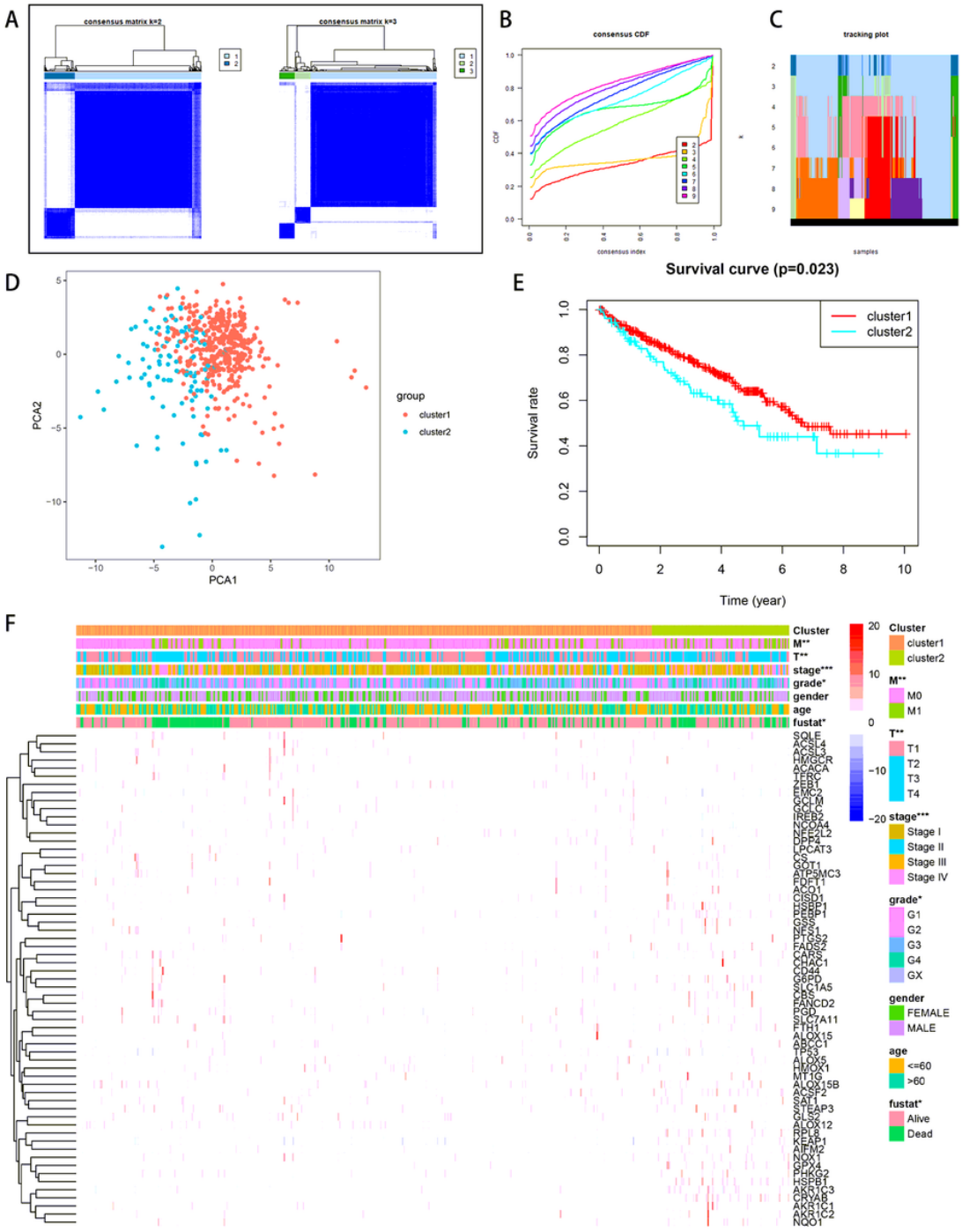

Figure 2

Consensus clustering analysis of ferroptosis-related genes (FRGs) expression profiles of the KIRC patients in the TCGA dataset. (a) The consensus maps show the consensus clustering matrix for FRGs in the TCGA-KIRC dataset for k = 2, 3. The optimal clustering is represented by k=2. (b) Consensus clustering cumulative distribution function (CDF) for k = 2 to 9. (c) The tracking plot for k = 2 to 9. (d) Principal component analysis demonstrates the gene expression differences between two patient clusters (cluster1 and cluster2). (e) The overall survival in the cluster 2 is significantly shorter than that in the cluster 1. (f) Heatmap shows the correlation between the expression of FRGs and the clinicopathological features of the two KIRC patient clusters. * P<0.05; ** P<0.01; *** P<0.001.

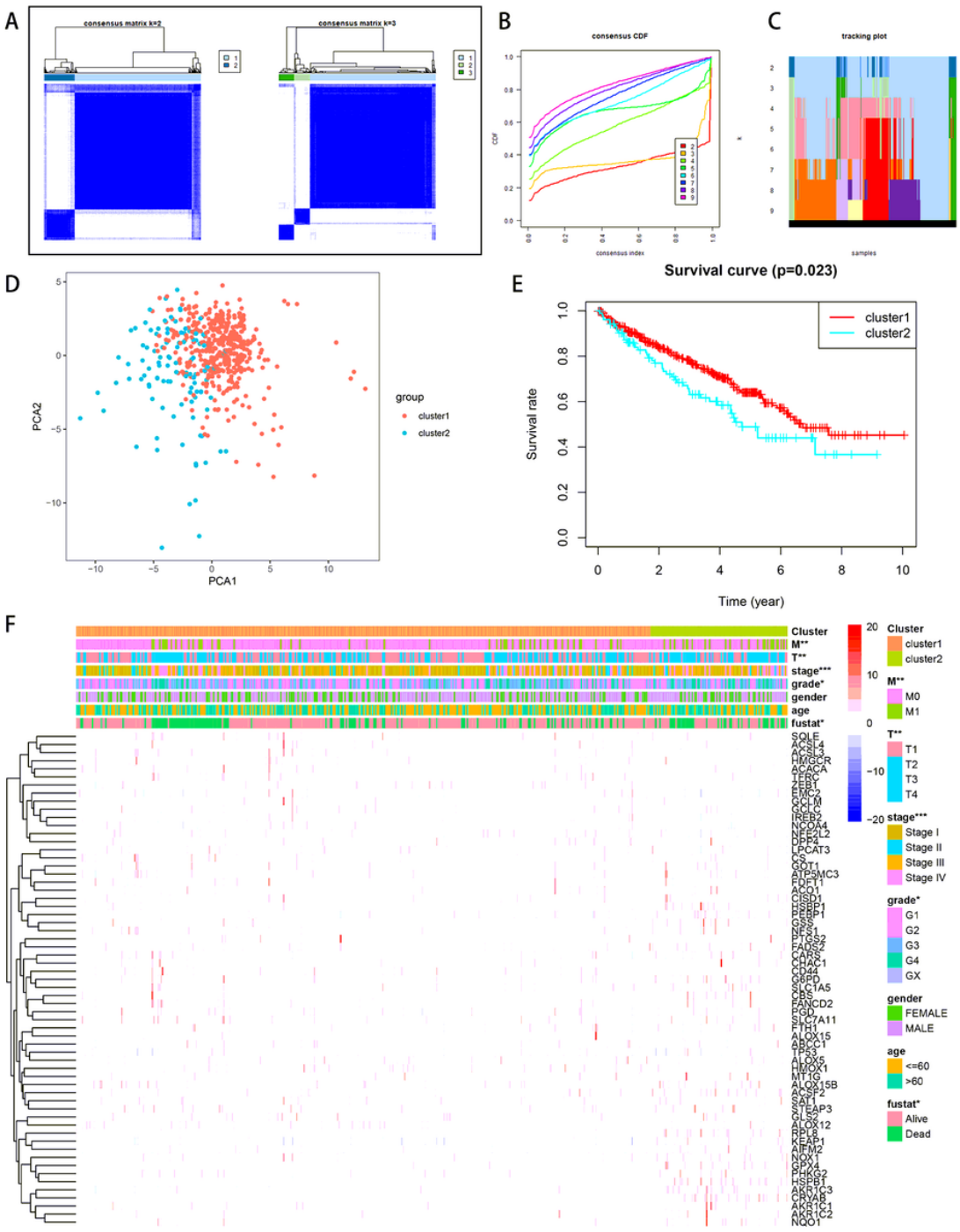

Figure 2

Consensus clustering analysis of ferroptosis-related genes (FRGs) expression profiles of the KIRC patients in the TCGA dataset. (a) The consensus maps show the consensus clustering matrix for FRGs in the TCGA-KIRC dataset for k = 2, 3. The optimal clustering is represented by k=2. (b) Consensus clustering cumulative distribution function (CDF) for k = 2 to 9. (c) The tracking plot for k = 2 to 9. (d) Principal component analysis demonstrates the gene expression differences between two patient clusters (cluster1 and cluster2). (e) The overall survival in the cluster 2 is significantly shorter than that in the cluster 1. (f) Heatmap shows the correlation between the expression of FRGs and the clinicopathological features of the two KIRC patient clusters. * P<0.05; ** P<0.01; *** P<0.001.

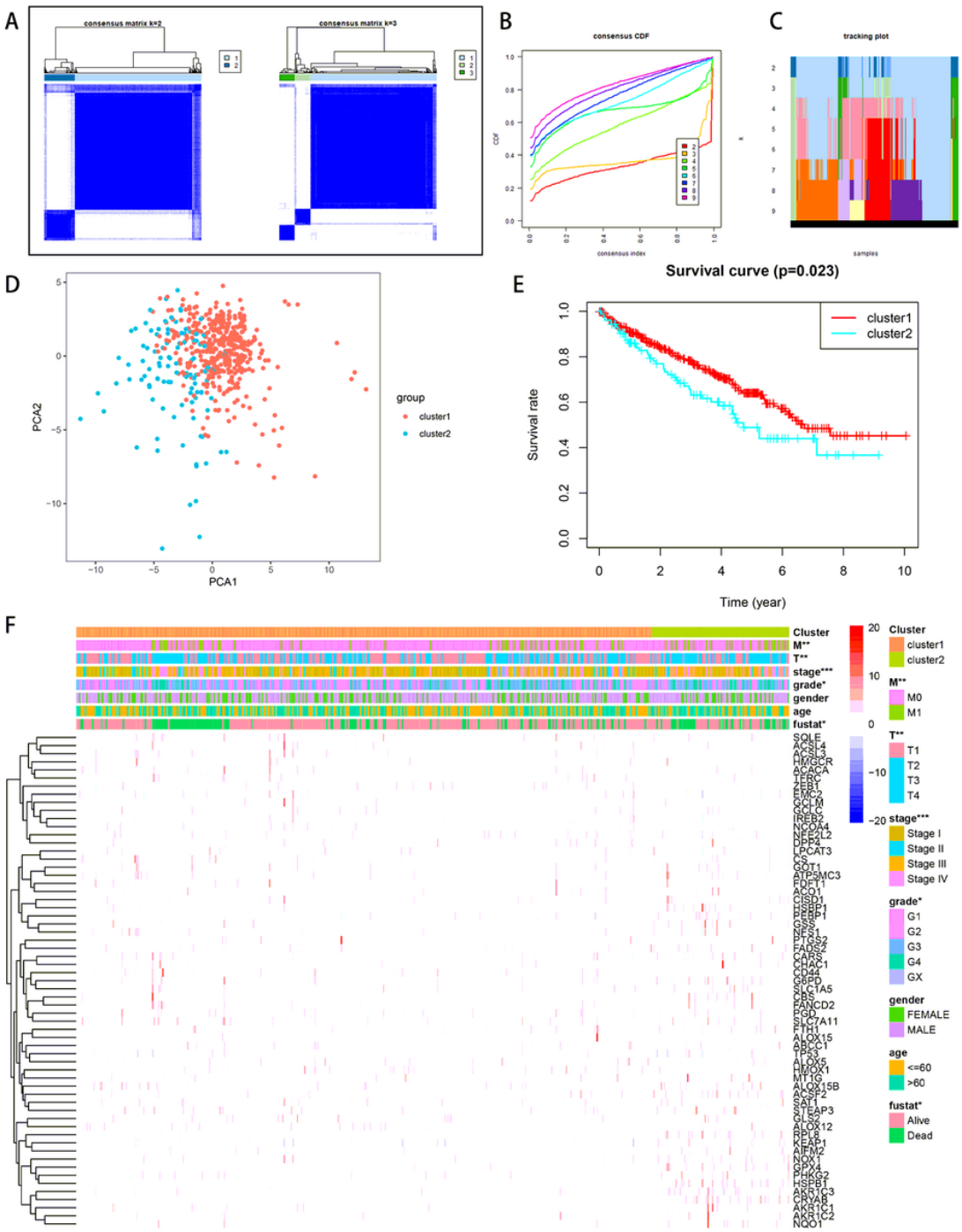

Figure 2

Consensus clustering analysis of ferroptosis-related genes (FRGs) expression profiles of the KIRC patients in the TCGA dataset. (a) The consensus maps show the consensus clustering matrix for FRGs in the TCGA-KIRC dataset for k = 2, 3. The optimal clustering is represented by k=2. (b) Consensus clustering cumulative distribution function (CDF) for k = 2 to 9. (c) The tracking plot for k = 2 to 9. (d) Principal component analysis demonstrates the gene expression differences between two patient clusters (cluster1 and cluster2). (e) The overall survival in the cluster 2 is significantly shorter than that in the cluster 1. (f) Heatmap shows the correlation between the expression of FRGs and the clinicopathological features of the two KIRC patient clusters. * P<0.05; ** P<0.01; *** P<0.001.

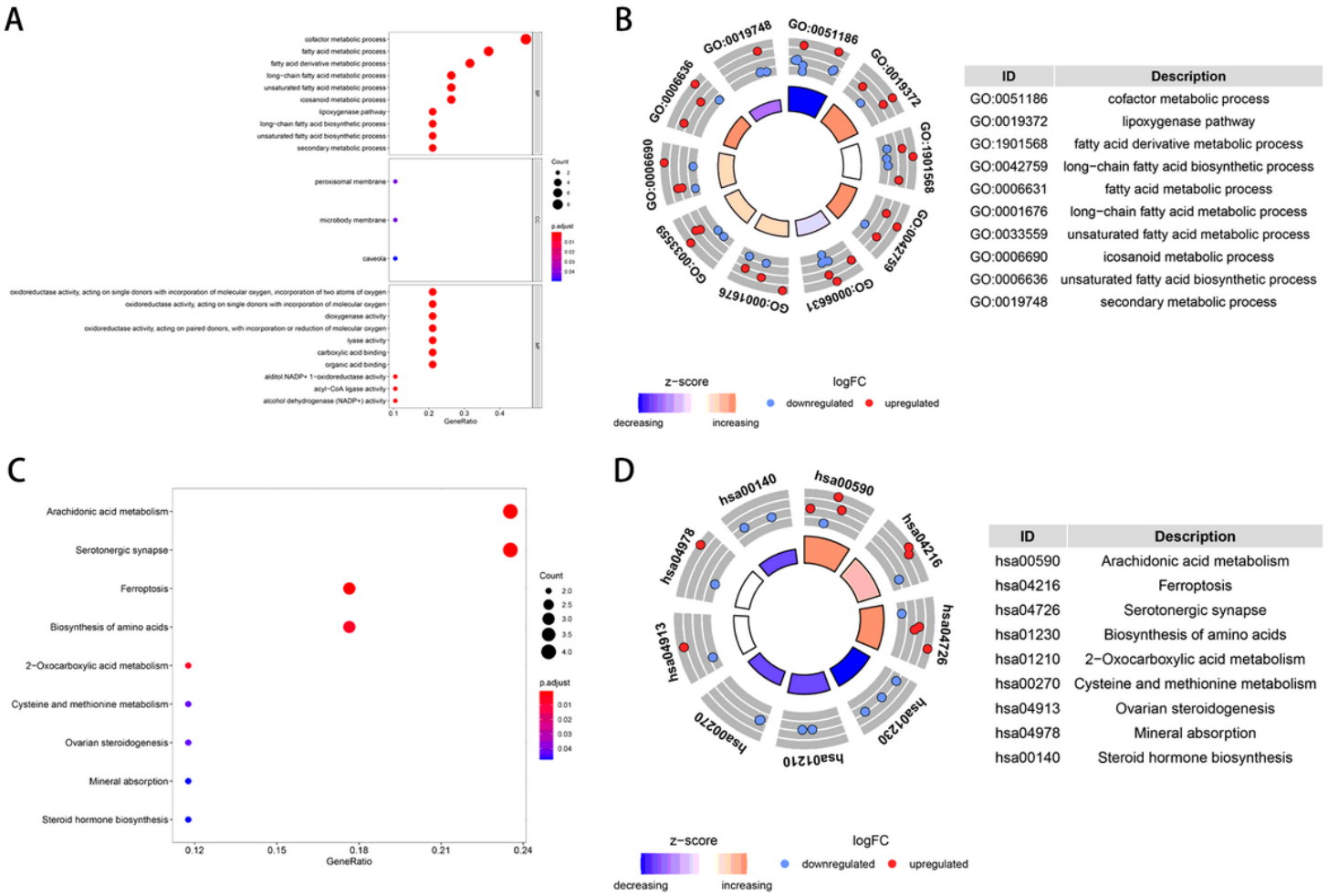

ID	Description
GO:0051186	cofactor metabolic process
GO:0019372	lipoxygenase pathway
GO:1901568	fatty acid derivative metabolic process
GO:0042759	long−chain fatty acid biosynthetic process
GO:0006631	fatty acid metabolic process
GO:0001676	long−chain fatty acid metabolic process
GO:0033559	unsaturated fatty acid metabolic process
GO:0006690	icosanoid metabolic process
GO:0006636	unsaturated fatty acid biosynthetic process
GO:0019748	secondary metabolic process

ID	Description
hsa00590	Arachidonic acid metabolism
hsa04216	Ferroptosis
hsa04726	Serotonergic synapse
hsa01230	Biosynthesis of amino acids
hsa01210	2−Oxocarboxylic acid metabolism
hsa00270	Cysteine and methionine metabolism
hsa04913	Ovarian steroidogenesis
hsa04978	Mineral absorption
hsa00140	Steroid hormone biosynthesis

Figure 3

GO and KEGG functional annotation analyses of 19 differentially expressed ferroptosis-related genes. (a) Bubble chart of significantly enriched GO term. BP indicates biological process, CC indicates cellular component, and MF indicates molecular function. (b) The circle shows the scatter map of the specified gene in each GO term. The red circles and blue circles represent up-regulation and down-regulation genes, respectively. The higher the Z-score value, the higher the enrichment pathway expression. (c) Bubble chart of significantly enriched KEGG pathways. (d) The circle shows the scatter map of the specified gene in each KEGG pathways. The red circles and blue circles represent up-regulation and down-regulation genes, respectively. The higher the Z-score value, the higher the enrichment pathway expression.

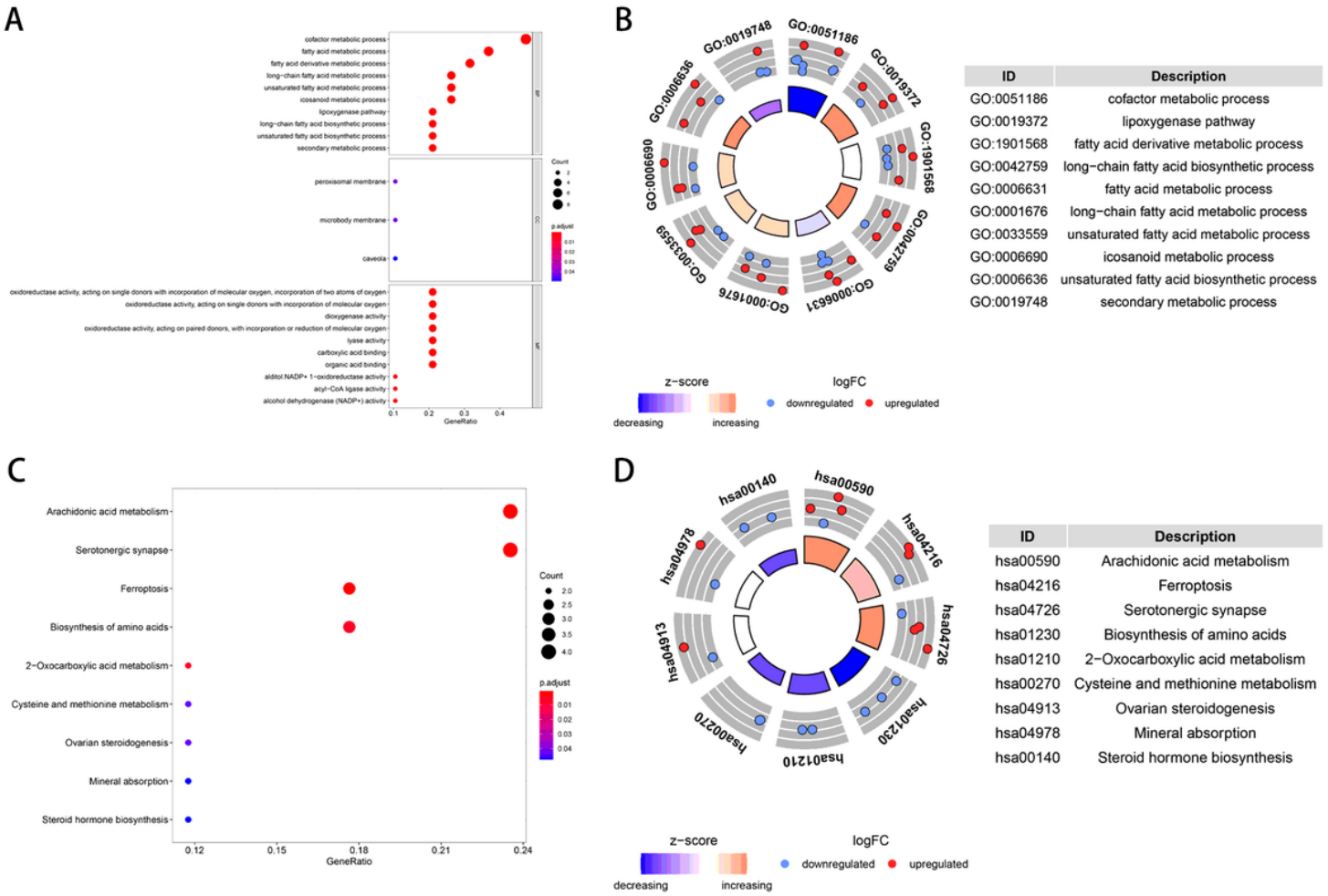

ID	Description
GO:0051186	cofactor metabolic process
GO:0019372	lipoxygenase pathway
GO:1901568	fatty acid derivative metabolic process
GO:0042759	long−chain fatty acid biosynthetic process
GO:0006631	fatty acid metabolic process
GO:0001676	long−chain fatty acid metabolic process
GO:0033559	unsaturated fatty acid metabolic process
GO:0006690	icosanoid metabolic process
GO:0006636	unsaturated fatty acid biosynthetic process
GO:0019748	secondary metabolic process

ID	Description
hsa00590	Arachidonic acid metabolism
hsa04216	Ferroptosis
hsa04726	Serotonergic synapse
hsa01230	Biosynthesis of amino acids
hsa01210	2−Oxocarboxylic acid metabolism
hsa00270	Cysteine and methionine metabolism
hsa04913	Ovarian steroidogenesis
hsa04978	Mineral absorption
hsa00140	Steroid hormone biosynthesis

Figure 3

GO and KEGG functional annotation analyses of 19 differentially expressed ferroptosis-related genes. (a) Bubble chart of significantly enriched GO term. BP indicates biological process, CC indicates cellular component, and MF indicates molecular function. (b) The circle shows the scatter map of the specified gene in each GO term. The red circles and blue circles represent up-regulation and down-regulation genes, respectively. The higher the Z-score value, the higher the enrichment pathway expression. (c) Bubble chart of significantly enriched KEGG pathways. (d) The circle shows the scatter map of the specified gene in each KEGG pathways. The red circles and blue circles represent up-regulation and down-regulation genes, respectively. The higher the Z-score value, the higher the enrichment pathway expression.

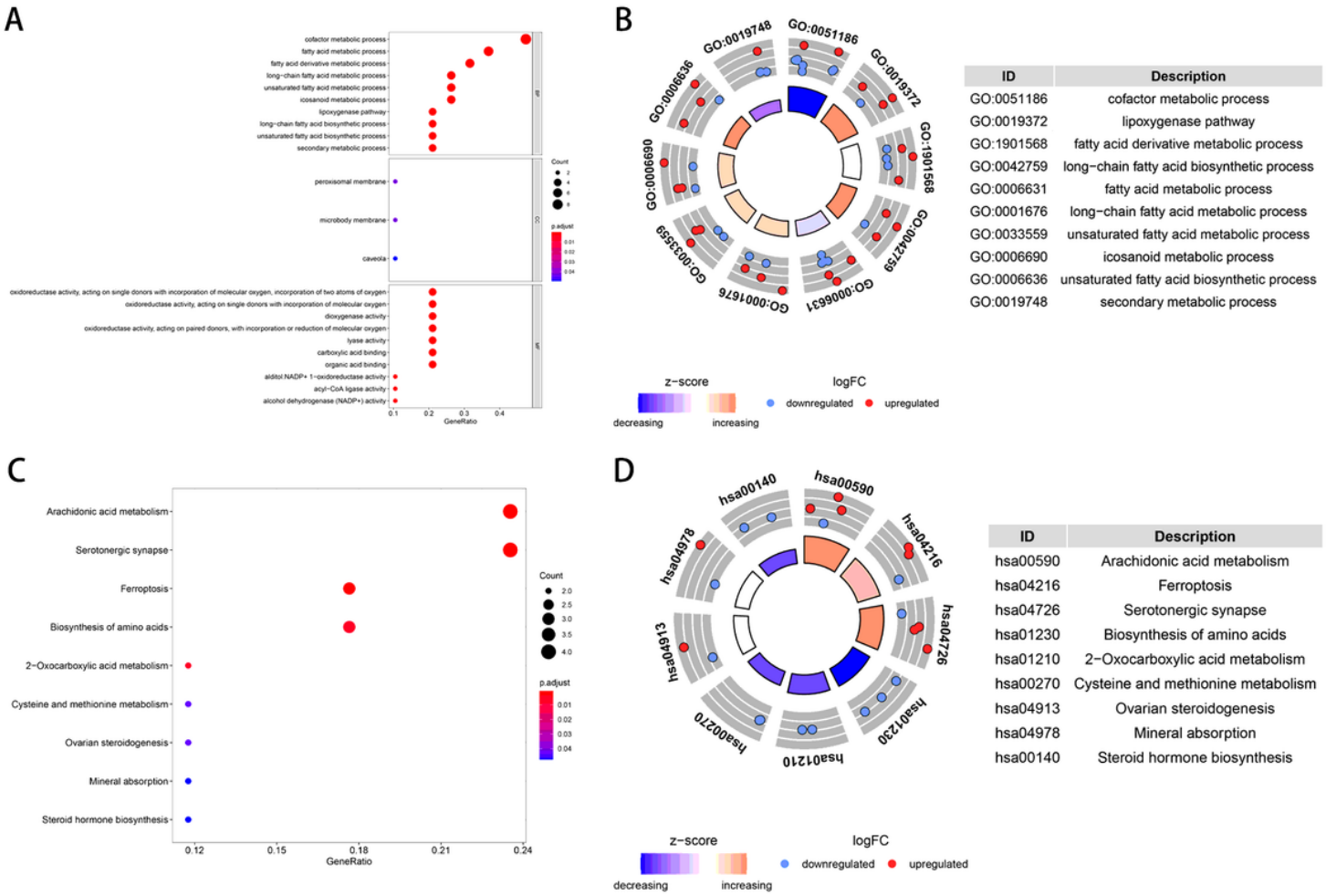

ID	Description
GO:0051186	cofactor metabolic process
GO:0019372	lipoxygenase pathway
GO:1901568	fatty acid derivative metabolic process
GO:0042759	long−chain fatty acid biosynthetic process
GO:0006631	fatty acid metabolic process
GO:0001676	long−chain fatty acid metabolic process
GO:0033559	unsaturated fatty acid metabolic process
GO:0006690	icosanoid metabolic process
GO:0006636	unsaturated fatty acid biosynthetic process
GO:0019748	secondary metabolic process

ID	Description
hsa00590	Arachidonic acid metabolism
hsa04216	Ferroptosis
hsa04726	Serotonergic synapse
hsa01230	Biosynthesis of amino acids
hsa01210	2−Oxocarboxylic acid metabolism
hsa00270	Cysteine and methionine metabolism
hsa04913	Ovarian steroidogenesis
hsa04978	Mineral absorption
hsa00140	Steroid hormone biosynthesis

Figure 3

GO and KEGG functional annotation analyses of 19 differentially expressed ferroptosis-related genes. (a) Bubble chart of significantly enriched GO term. BP indicates biological process, CC indicates cellular component, and MF indicates molecular function. (b) The circle shows the scatter map of the specified gene in each GO term. The red circles and blue circles represent up-regulation and down-regulation genes, respectively. The higher the Z-score value, the higher the enrichment pathway expression. (c) Bubble chart of significantly enriched KEGG pathways. (d) The circle shows the scatter map of the specified gene in each KEGG pathways. The red circles and blue circles represent up-regulation and down-regulation genes, respectively. The higher the Z-score value, the higher the enrichment pathway expression.

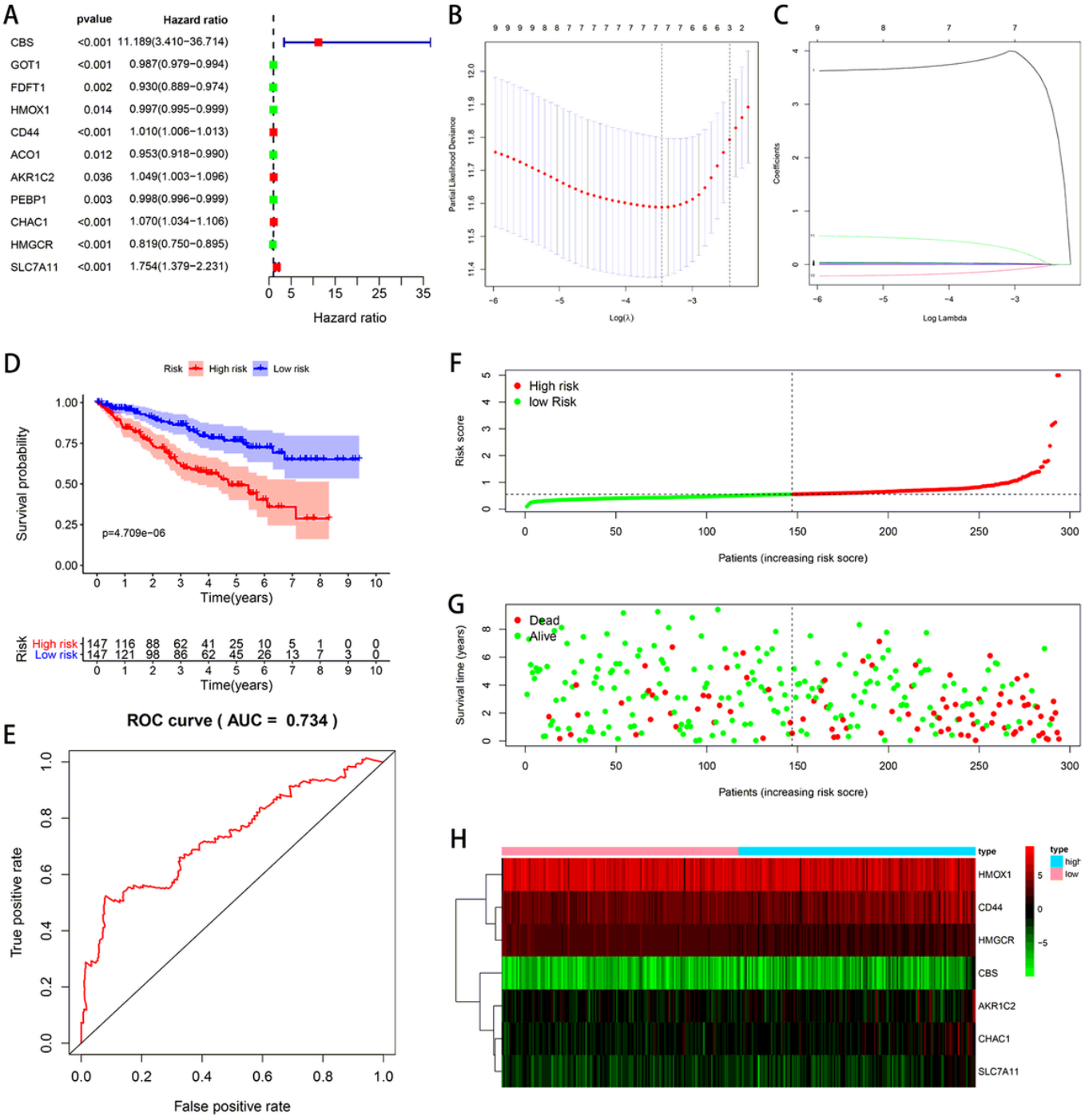

Figure 4

Construction and evaluation of a prognostic signature based on seven ferroptosis-related genes (FRGs) in the training cohort of KIRC patients. (a) Univariate Cox analysis reveals 11 candidate prognosis-related FRGs. (b) The optimal penalty parameter (λ) at the vertical line is selected following the minimum criteria (left). (c) Lasso coefficient profiles of the 11 candidate prognosis-related FRGs. (d) Kaplan-Meier overall survival curves for KIRC patients shows that the high-risk group had significantly shorter OS than the low-risk group. (e) ROC curve demonstrates the veracity and reliability for the prognostic signature. (f) Risk score distribution of TCGA-KIRC patients. (g) The distributions of risk scores and the survival status. (h) The heatmap displays that the expression levels of the seven FRGs in the high- and low-risk groups.

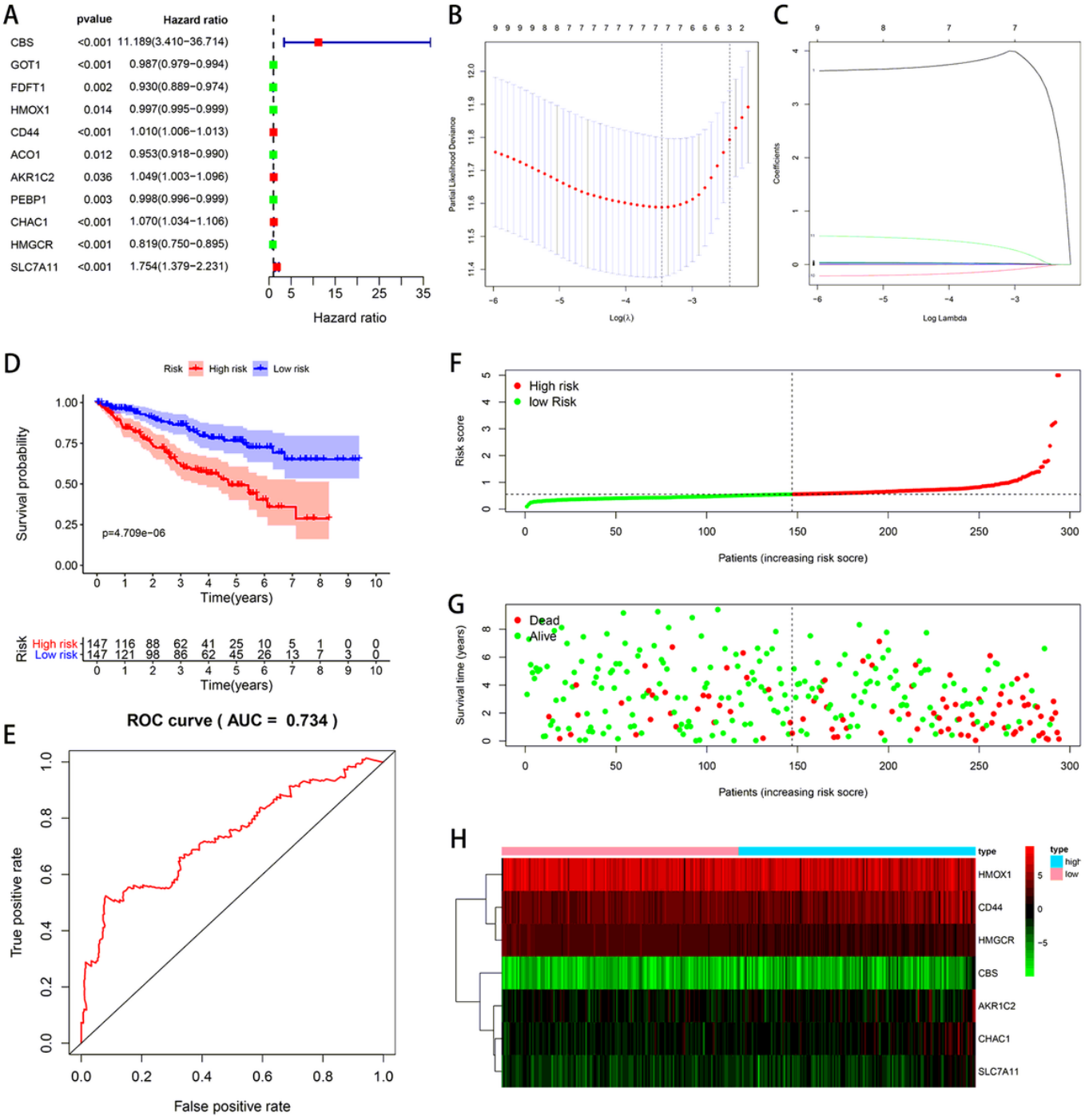

Figure 4

Construction and evaluation of a prognostic signature based on seven ferroptosis-related genes (FRGs) in the training cohort of KIRC patients. (a) Univariate Cox analysis reveals 11 candidate prognosis-related FRGs. (b) The optimal penalty parameter (λ) at the vertical line is selected following the minimum criteria (left). (c) Lasso coefficient profiles of the 11 candidate prognosis-related FRGs. (d) Kaplan-Meier overall survival curves for KIRC patients shows that the high-risk group had significantly shorter OS than the low-risk group. (e) ROC curve demonstrates the veracity and reliability for the prognostic signature. (f) Risk score distribution of TCGA-KIRC patients. (g) The distributions of risk scores and the survival status. (h) The heatmap displays that the expression levels of the seven FRGs in the high- and low-risk groups.

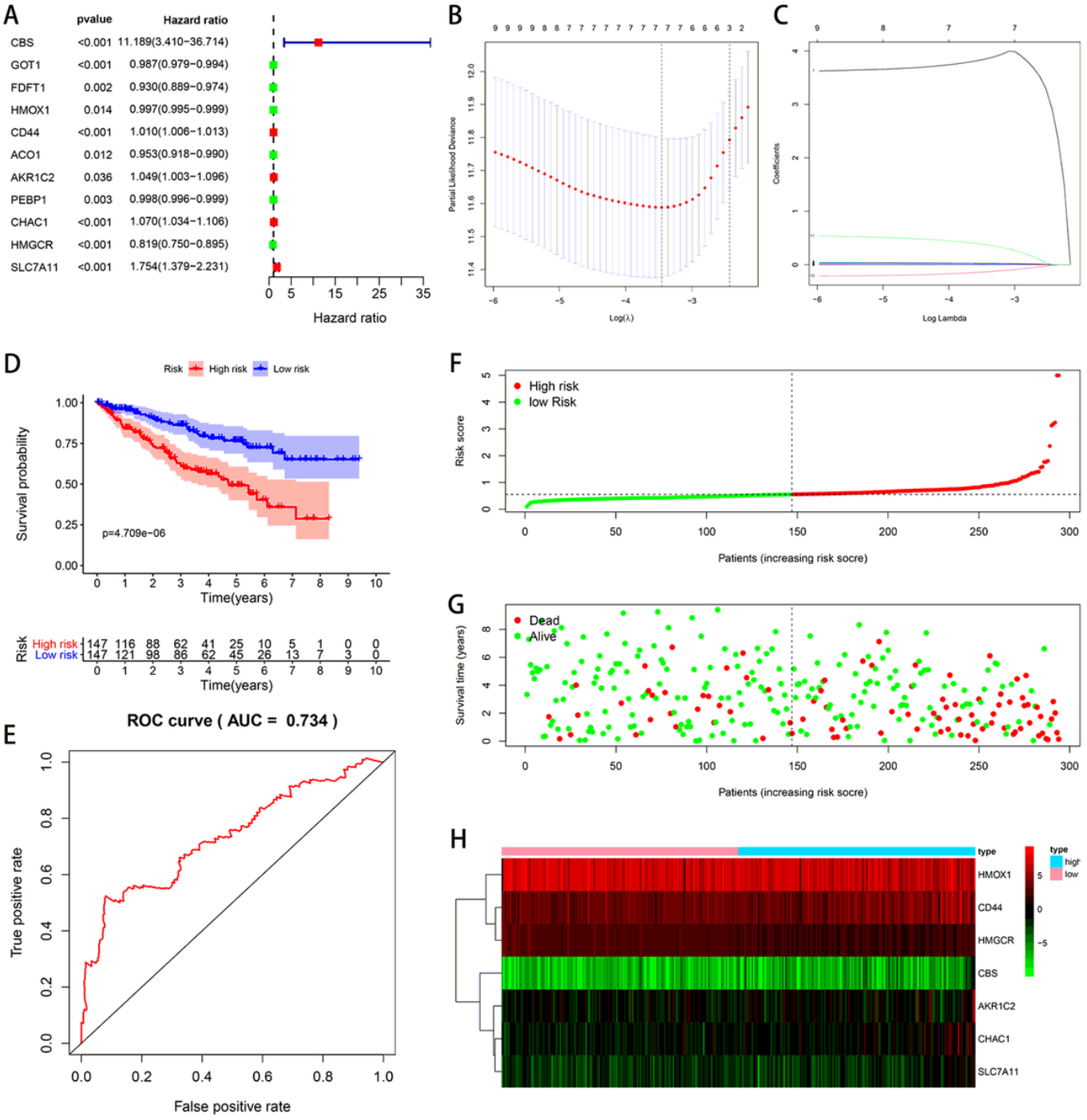

Figure 4

Construction and evaluation of a prognostic signature based on seven ferroptosis-related genes (FRGs) in the training cohort of KIRC patients. (a) Univariate Cox analysis reveals 11 candidate prognosis-related FRGs. (b) The optimal penalty parameter (λ) at the vertical line is selected following the minimum criteria (left). (c) Lasso coefficient profiles of the 11 candidate prognosis-related FRGs. (d) Kaplan-Meier overall survival curves for KIRC patients shows that the high-risk group had significantly shorter OS than the low-risk group. (e) ROC curve demonstrates the veracity and reliability for the prognostic signature. (f) Risk score distribution of TCGA-KIRC patients. (g) The distributions of risk scores and the survival status. (h) The heatmap displays that the expression levels of the seven FRGs in the high- and low-risk groups.

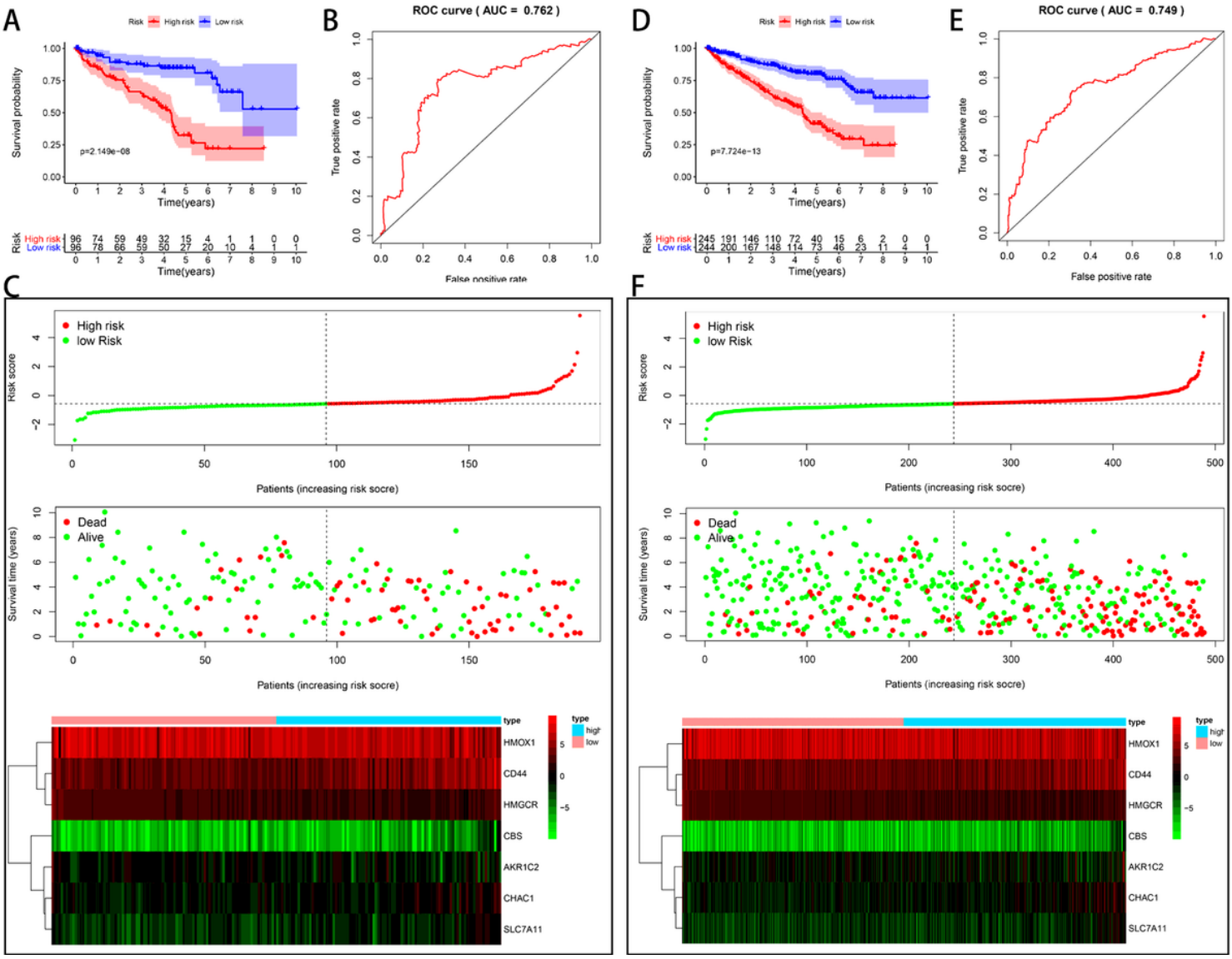

Figure 5

Validation of the prognostic risk signature in the testing cohort and entire cohort of KIRC patients. Kaplan-Meier curve analysis of high-risk and low-risk patients in the testing cohort (a) and the entire TCGA cohort (d). ROC curve analysis of the testing cohort (b) and the entire TCGA cohort (e). The risk score distribution, survival status and risk gene expression in the testing cohort (c) and the entire TCGA cohort (f).

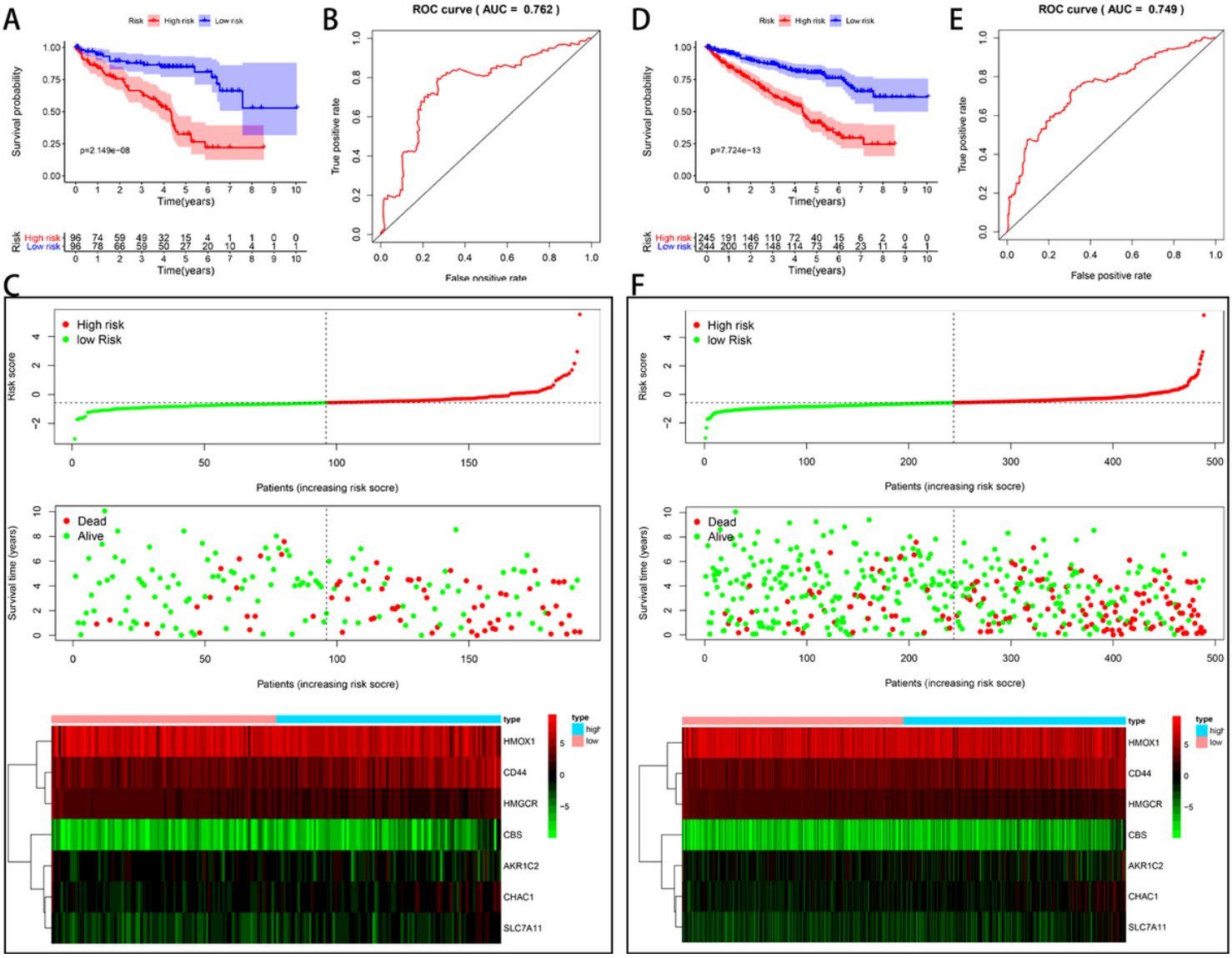

Figure 5

Validation of the prognostic risk signature in the testing cohort and entire cohort of KIRC patients. Kaplan-Meier curve analysis of high-risk and low-risk patients in the testing cohort (a) and the entire TCGA cohort (d). ROC curve analysis of the testing cohort (b) and the entire TCGA cohort (e). The risk score distribution, survival status and risk gene expression in the testing cohort (c) and the entire TCGA cohort (f).

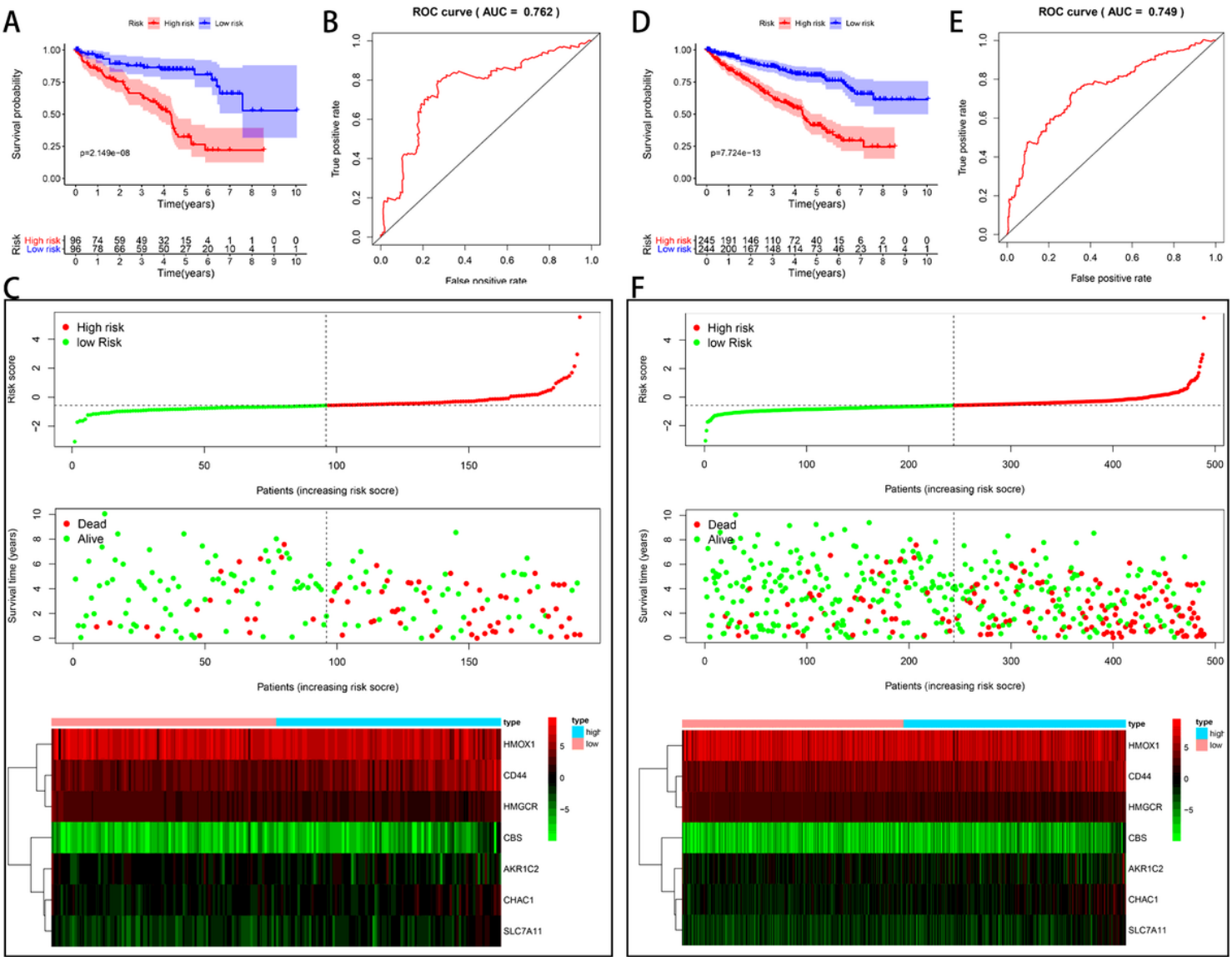

Figure 5

Validation of the prognostic risk signature in the testing cohort and entire cohort of KIRC patients. Kaplan-Meier curve analysis of high-risk and low-risk patients in the testing cohort (a) and the entire TCGA cohort (d). ROC curve analysis of the testing cohort (b) and the entire TCGA cohort (e). The risk score distribution, survival status and risk gene expression in the testing cohort (c) and the entire TCGA cohort (f).

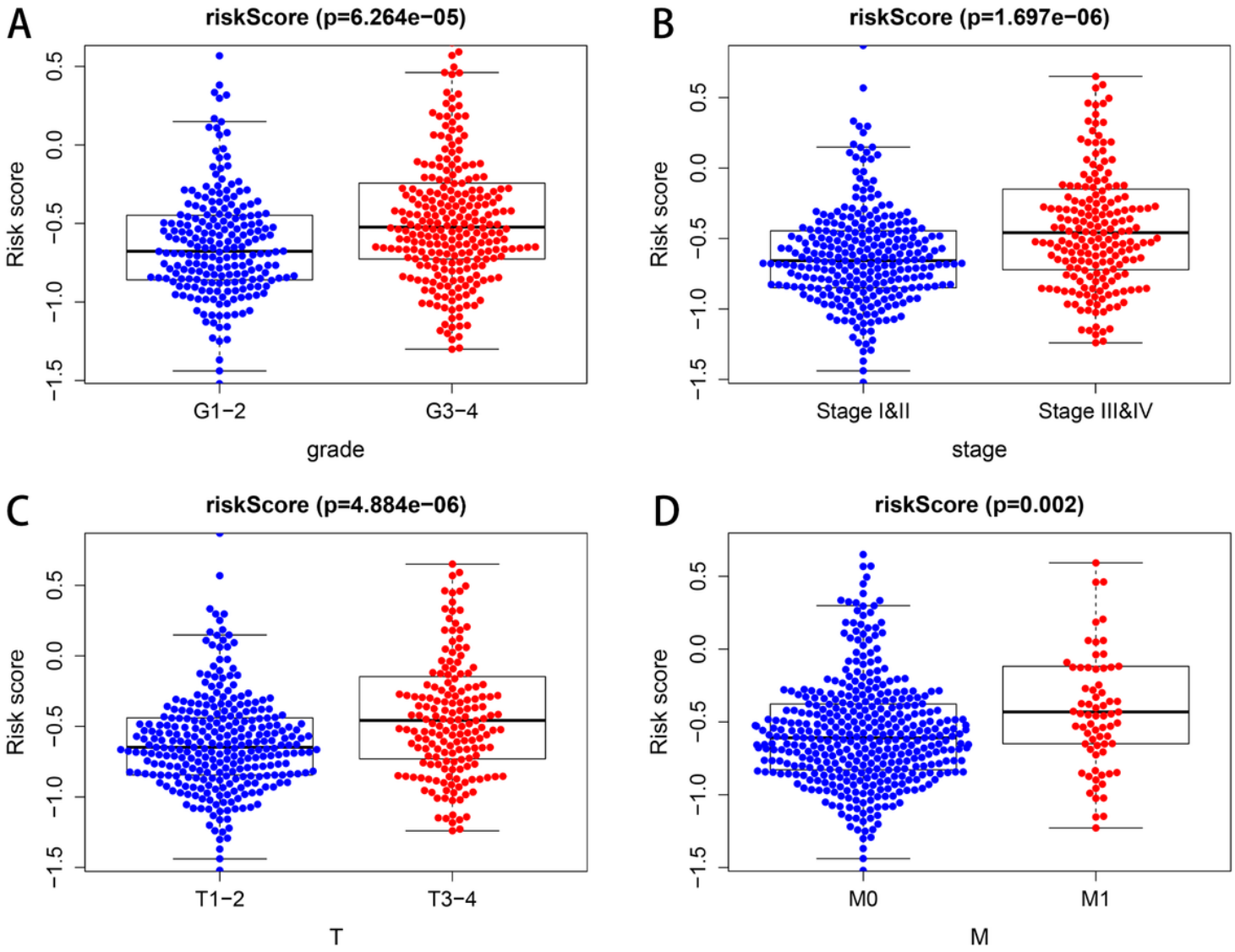

Figure 6

The relationship between the risk score and different clinicopathological features. The distribution of risk scores in high- and low-risk patients stratified according to (a) Garde (G1-2 vs. G3-4), (b) AJCC stage (stages I-II vs. stages III-IV), (c) T stage (T1-2 vs. T3-4), and (d) M stage (M0 vs. M1).

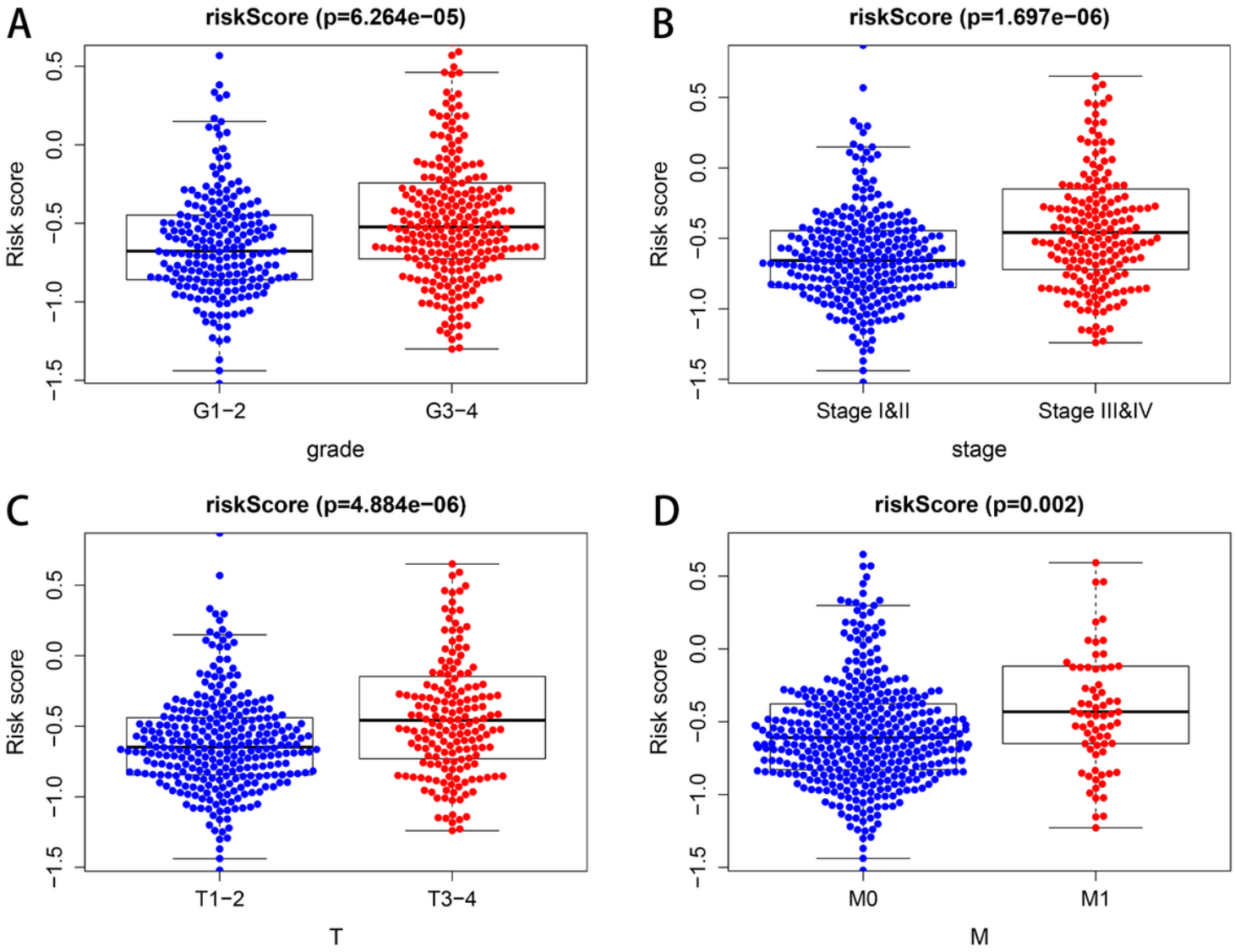

Figure 6

The relationship between the risk score and different clinicopathological features. The distribution of risk scores in high- and low-risk patients stratified according to (a) Garde (G1-2 vs. G3-4), (b) AJCC stage (stages I-II vs. stages III-IV), (c) T stage (T1-2 vs. T3-4), and (d) M stage (M0 vs. M1).

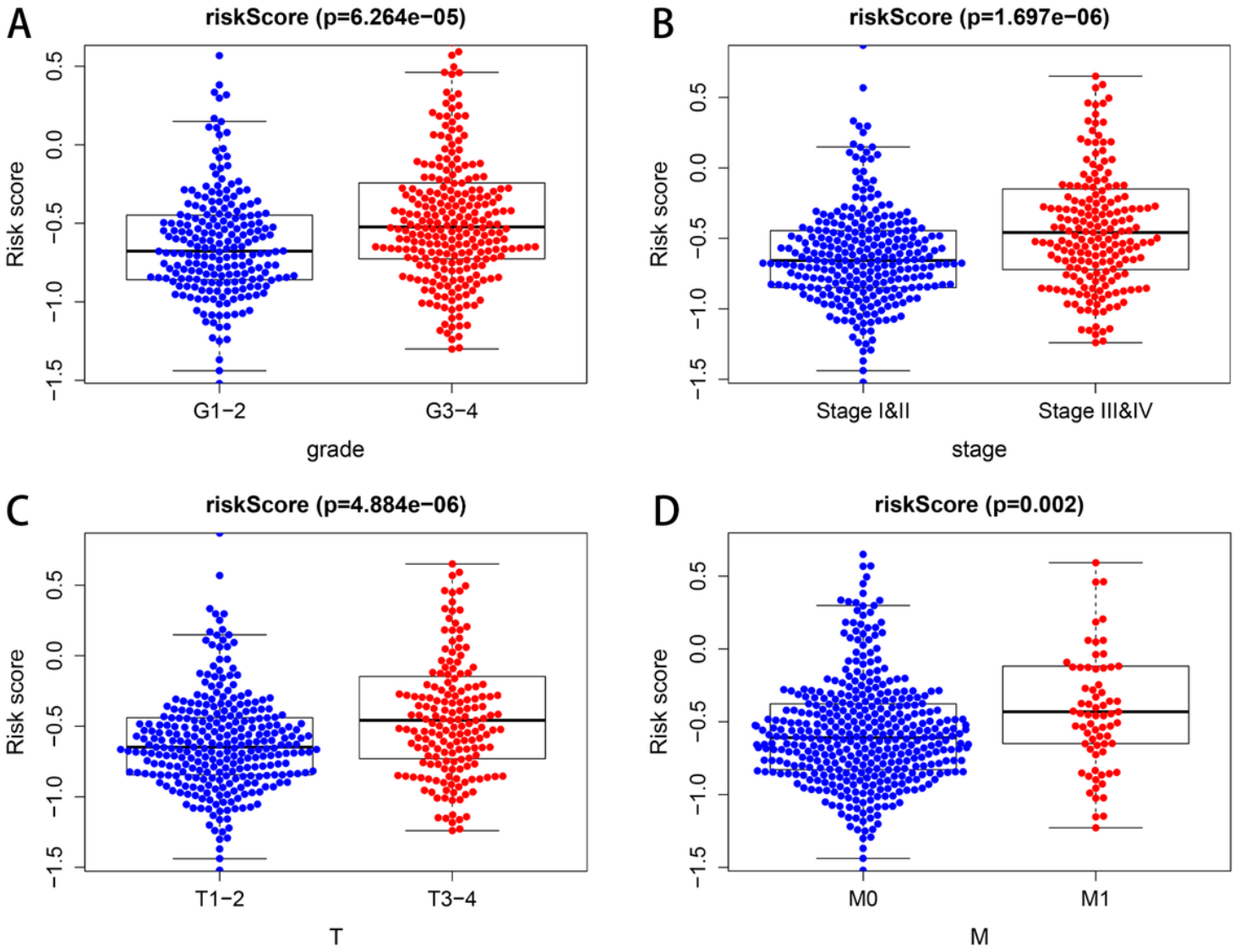

Figure 6

The relationship between the risk score and different clinicopathological features. The distribution of risk scores in high- and low-risk patients stratified according to (a) Garde (G1-2 vs. G3-4), (b) AJCC stage (stages I-II vs. stages III-IV), (c) T stage (T1-2 vs. T3-4), and (d) M stage (M0 vs. M1).

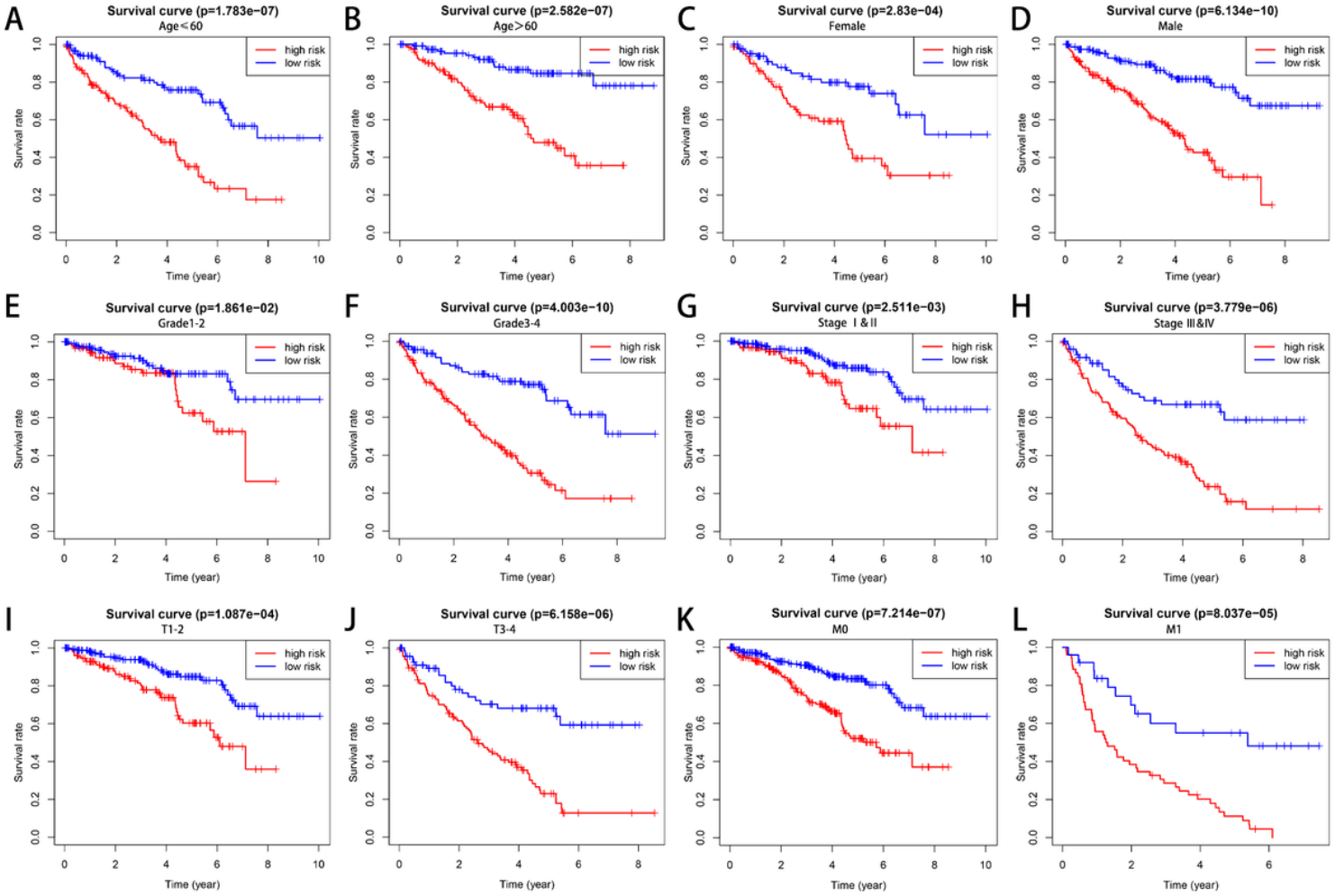

Figure 7

The overall survival (OS) rates in high- and low-risk KIRC patients stratified by clinicopathological parameters. Kaplan-Meier survival curve analysis shows the OS rates of high-and low-risk KIRC patients from the TCGA database stratified by (a, b) age (≤ 60 and > 60), (c, d) gender (female and male), (e, f) grade (G1-2 and G3-4), (g, h) AJCC stages (stages Ⅰ/Ⅱ and Ⅲ/Ⅳ), (I, j) T stages (T1-2 and T3-4), and (k, l) M stages (M0 and M1).

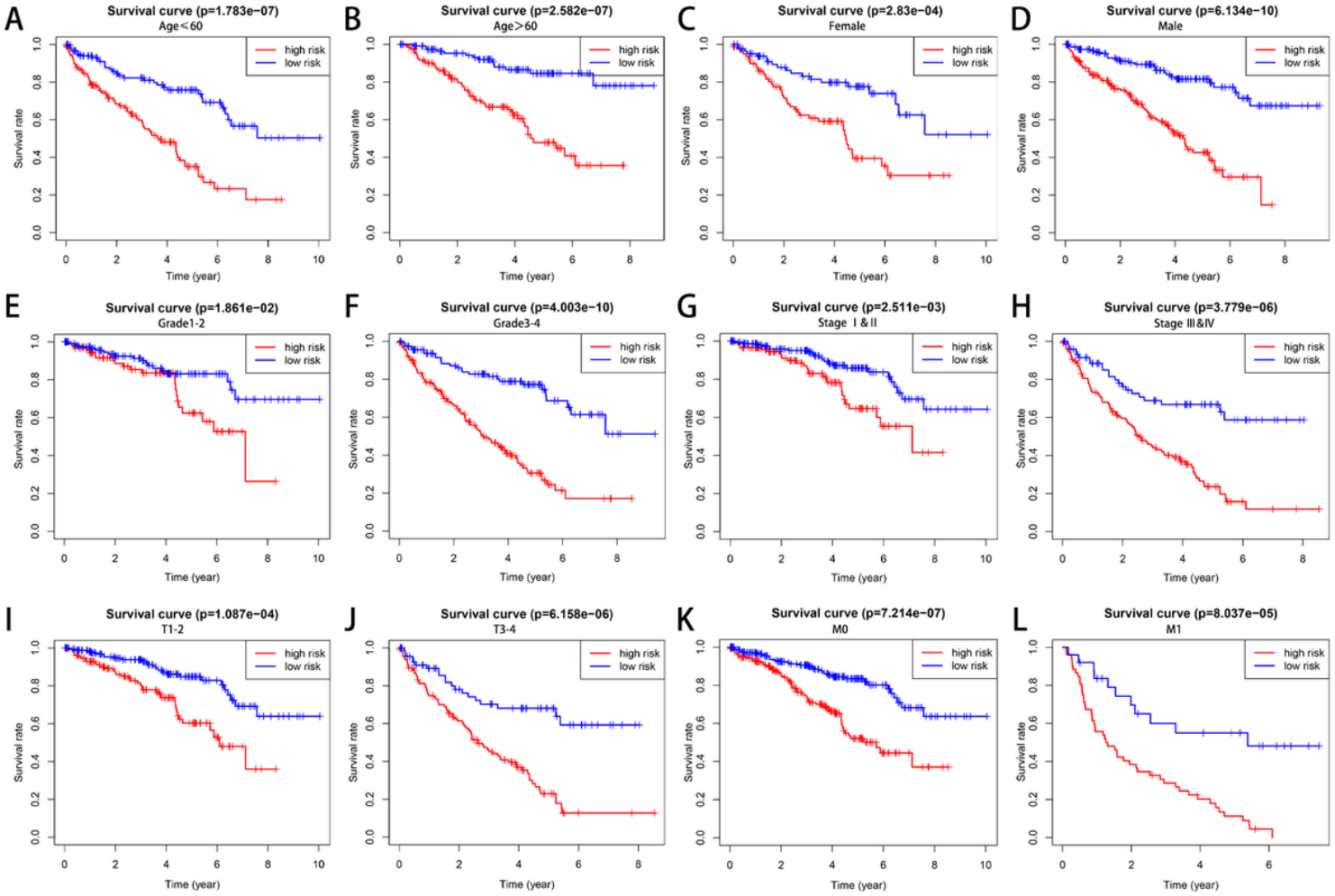

Figure 7

The overall survival (OS) rates in high- and low-risk KIRC patients stratified by clinicopathological parameters. Kaplan-Meier survival curve analysis shows the OS rates of high-and low-risk KIRC patients from the TCGA database stratified by (a, b) age (≤ 60 and > 60), (c, d) gender (female and male), (e, f) grade (G1-2 and G3-4), (g, h) AJCC stages (stages Ⅰ/Ⅱ and Ⅲ/Ⅳ), (I, j) T stages (T1-2 and T3-4), and (k, l) M stages (M0 and M1).

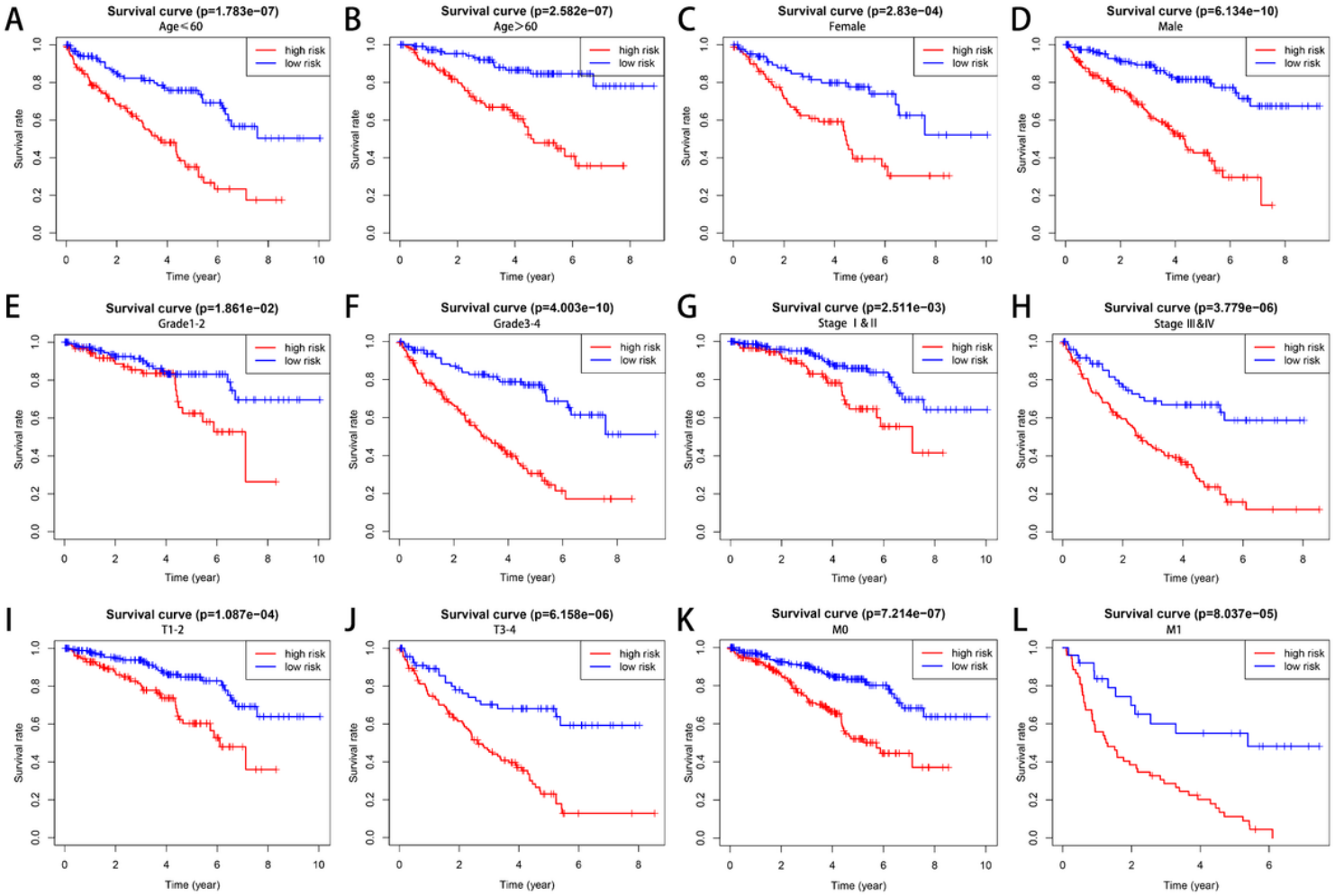

Figure 7

The overall survival (OS) rates in high- and low-risk KIRC patients stratified by clinicopathological parameters. Kaplan-Meier survival curve analysis shows the OS rates of high-and low-risk KIRC patients from the TCGA database stratified by (a, b) age (≤ 60 and > 60), (c, d) gender (female and male), (e, f) grade (G1-2 and G3-4), (g, h) AJCC stages (stages Ⅰ/Ⅱ and Ⅲ/Ⅳ), (I, j) T stages (T1-2 and T3-4), and (k, l) M stages (M0 and M1).

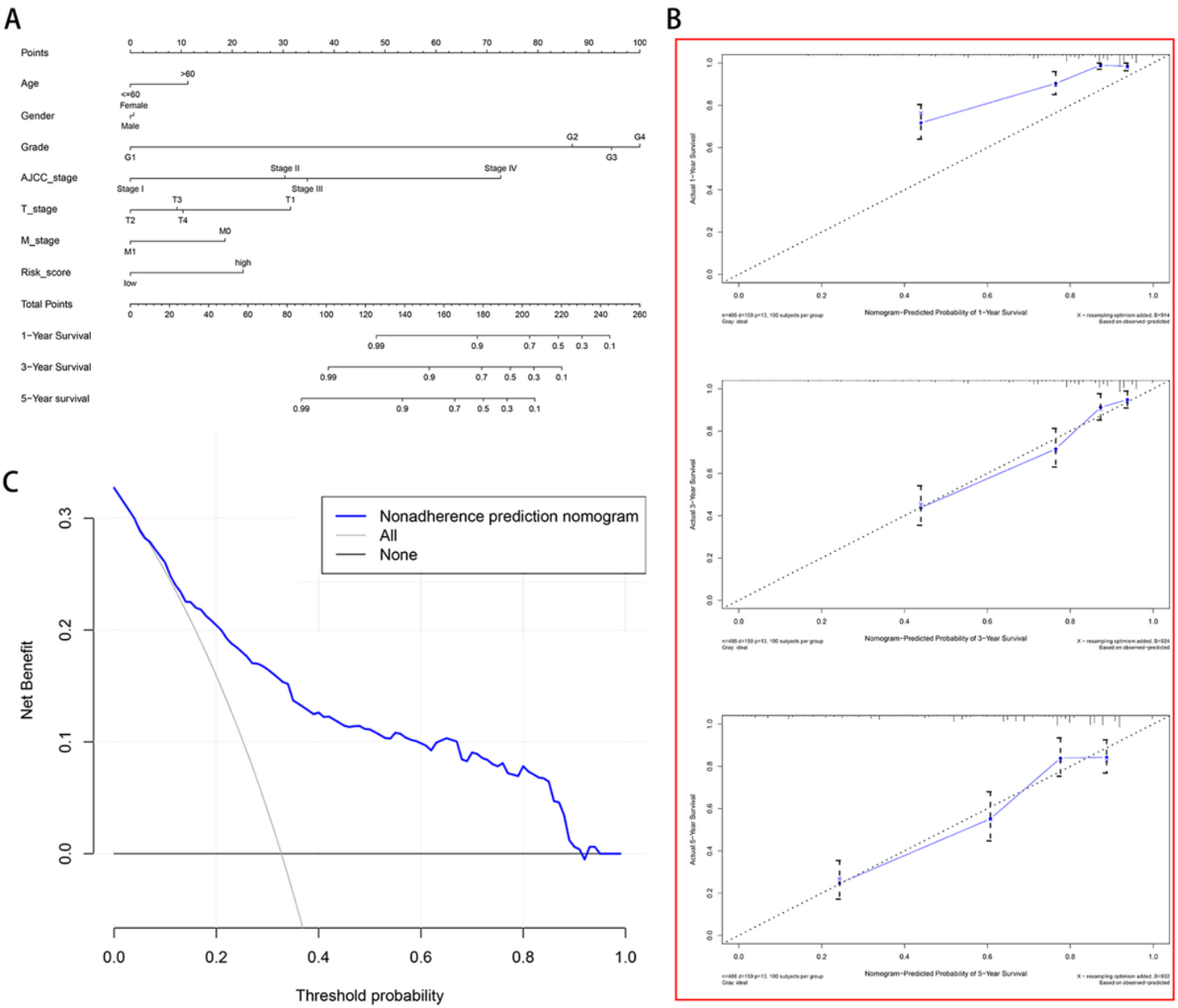

Figure 8

Development and validation of the nomogram predicting overall survival (OS) for KIRC patients in the TCGA cohort. (a) Prognostic nomogram for KIRC patients based on the constructed prognostic signature and clinicopathological parameters. (b) Calibration curves of the nomogram to predict OS at 1, 3, and 5 years. (c) The DCA curve of the nomogram.

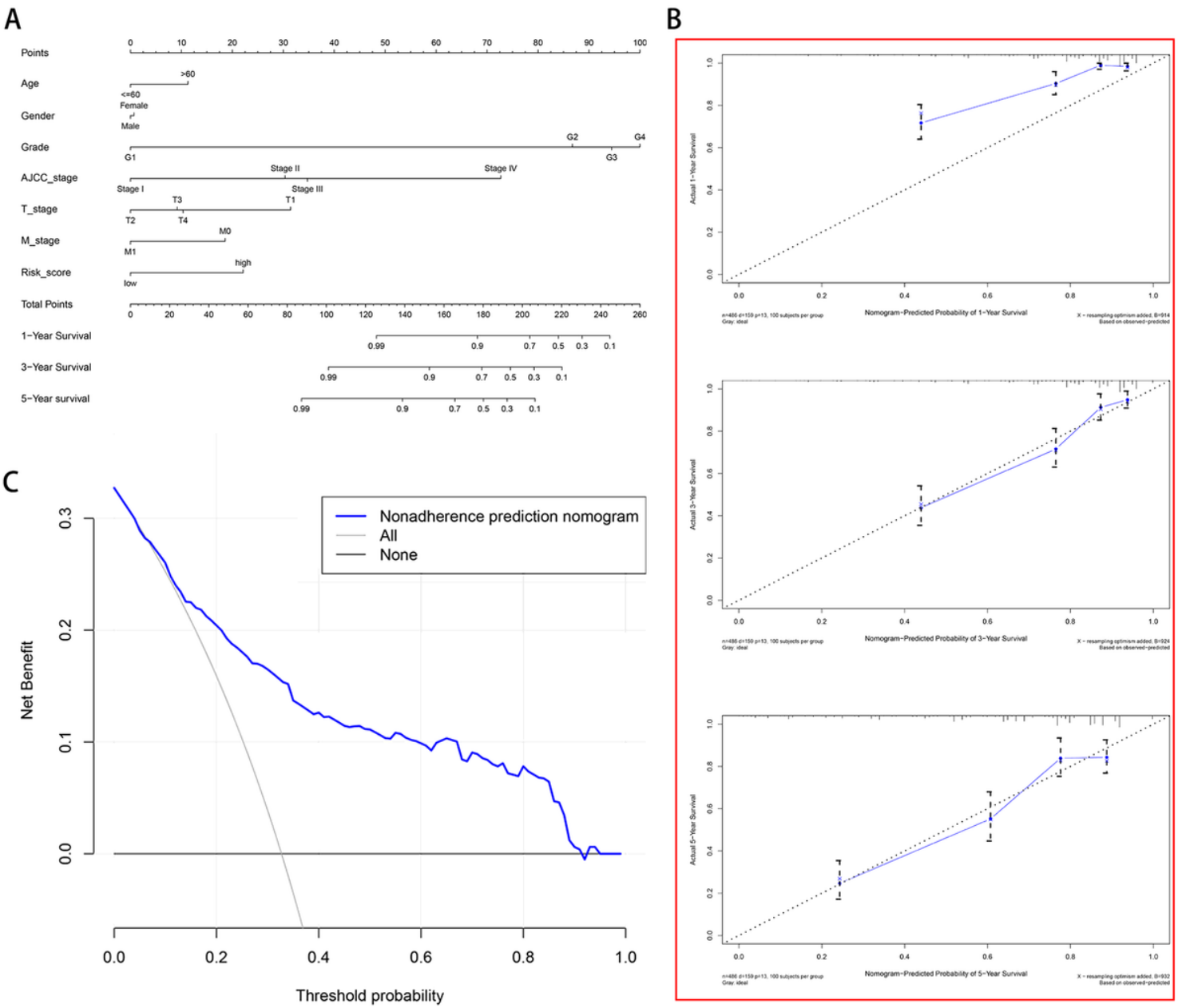

Figure 8

Development and validation of the nomogram predicting overall survival (OS) for KIRC patients in the TCGA cohort. (a) Prognostic nomogram for KIRC patients based on the constructed prognostic signature and clinicopathological parameters. (b) Calibration curves of the nomogram to predict OS at 1, 3, and 5 years. (c) The DCA curve of the nomogram.

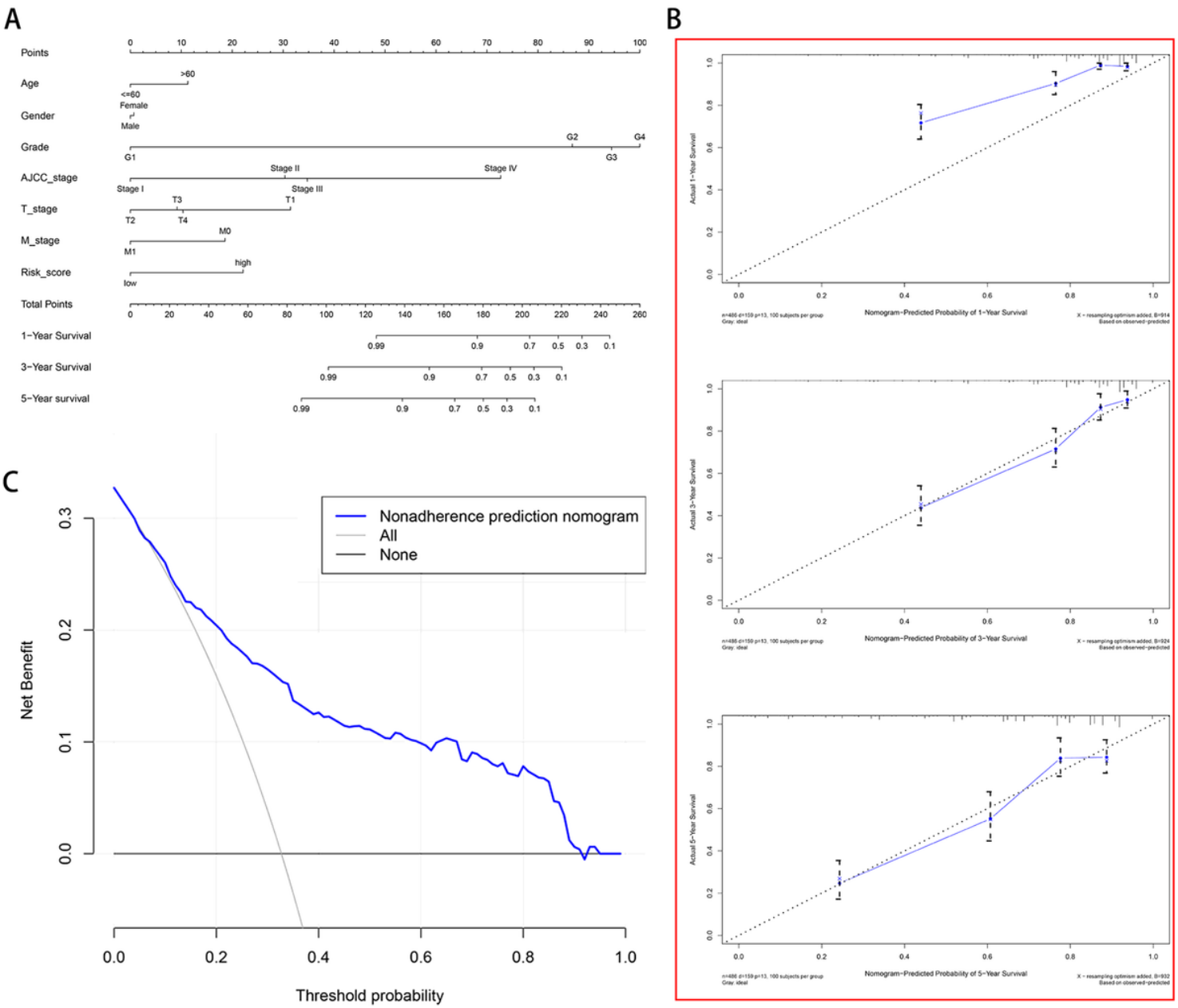

Figure 8

Development and validation of the nomogram predicting overall survival (OS) for KIRC patients in the TCGA cohort. (a) Prognostic nomogram for KIRC patients based on the constructed prognostic signature and clinicopathological parameters. (b) Calibration curves of the nomogram to predict OS at 1, 3, and 5 years. (c) The DCA curve of the nomogram.

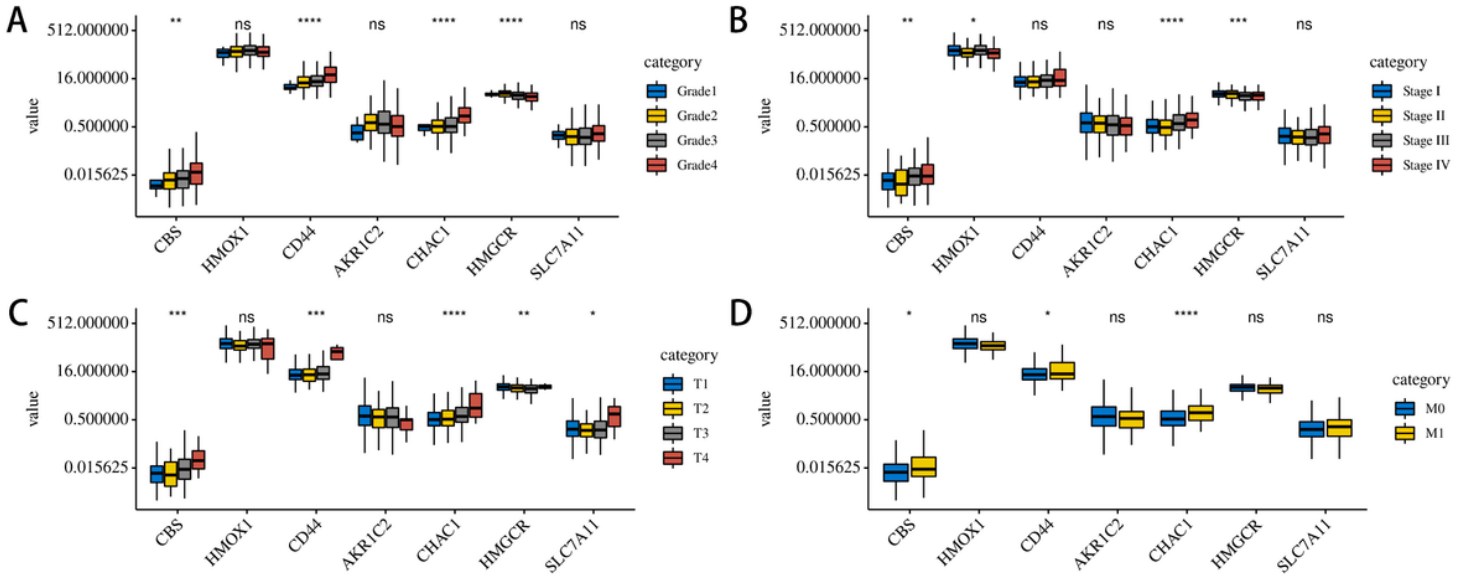

Figure 9

The expression patterns of the seven candidate ferroptosis-related genes (FRGs) in the TCGA-KIRC dataset. Expression of CBS, HMOX1, CD44, AKR1C2, CHAC1, HMGCR, and SLC7A11 in KIRC samples with different Grade (a), AJCC stage (b), T stage (c), and M grade (d).

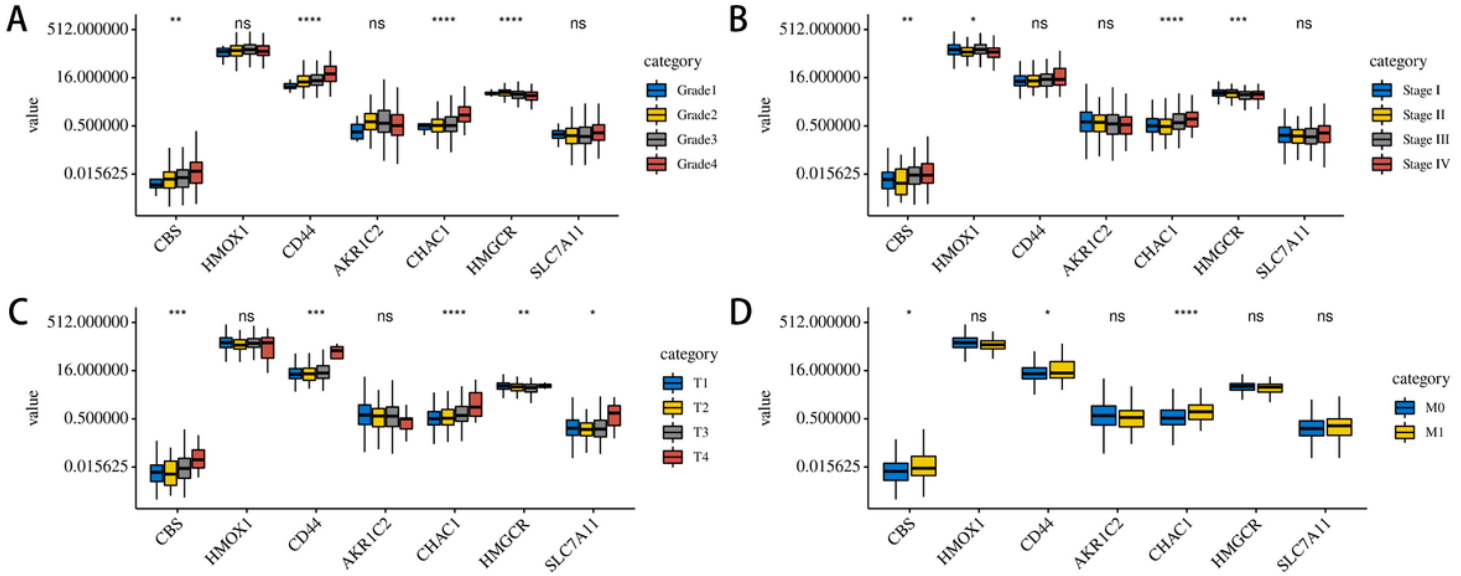

Figure 9

The expression patterns of the seven candidate ferroptosis-related genes (FRGs) in the TCGA-KIRC dataset. Expression of CBS, HMOX1, CD44, AKR1C2, CHAC1, HMGCR, and SLC7A11 in KIRC samples with different Grade (a), AJCC stage (b), T stage (c), and M grade (d).

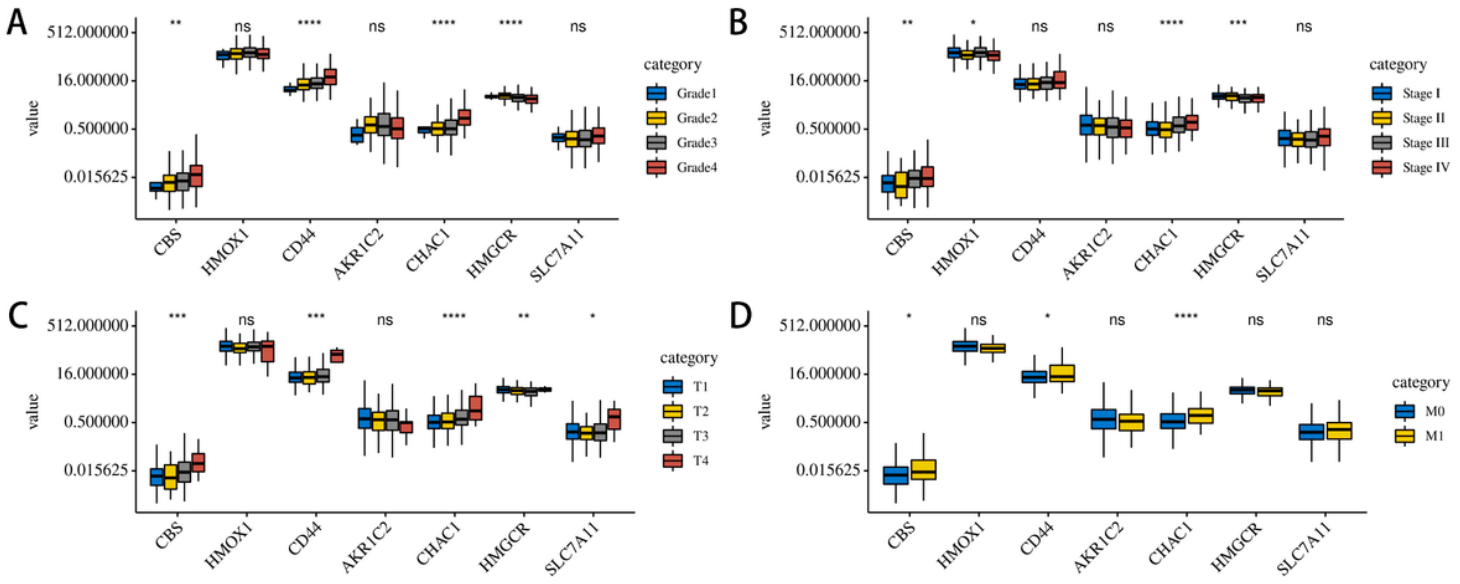

Figure 9

The expression patterns of the seven candidate ferroptosis-related genes (FRGs) in the TCGA-KIRC dataset. Expression of CBS, HMOX1, CD44, AKR1C2, CHAC1, HMGCR, and SLC7A11 in KIRC samples with different Grade (a), AJCC stage (b), T stage (c), and M grade (d).

Supplementary Files

This is a list of supplementary files associated with this preprint. Click to download.

- Supplementaryinformation.docx
- Supplementaryinformation.docx
- Supplementaryinformation.docx